DISSERTATIONS IN
FORESTRY AND
NATURAL SCIENCES

Tuomas Virén

Arthroscopic Ultrasound Imaging of Articular Cartilage

Publications of the University of Eastern Finland
Dissertations in Forestry and Natural Sciences

UNIVERSITY OF
EASTERN FINLAND

TUOMAS VIRÉN

Arthroscopic Ultrasound Imaging of Articular Cartilage

Publications of the University of Eastern Finland
Dissertations in Forestry and Natural Sciences
No 37

Academic Dissertation
To be presented by permission of the Faculty of Science and Forestry for public examination in the Auditorium L22 in Snellmania Building at the University of Eastern Finland, Kuopio, on June, 22, 2011,
at 12 o'clock noon.

Department of Applied Physics

Kopijyvä
Kuopio, 2011
Editor: Prof. Pertti Pasanen
Ph.D. Sinikka Parkkinen, Prof. Kai-Erik Peiponen

Distribution:
University of Eastern Finland Library / Sales of publications
P.O. Box 107, FI-80101 Joensuu, Finland
tel. +358-50-3058396
http://www.uef.fi/kirjasto

ISBN: 978-952-61-0470-6
ISBN: 978-952-61-0471-3 (PDF)
ISSNL: 1798-5668
ISSN: 1798-5668
ISSN: 1798-5676 (PDF)

Author's address:
University of Eastern Finland
Department of Applied Physics
P.O.Box 1627
70211 KUOPIO
FINLAND
email: Tuomas.Viren@uef.fi

Supervisors:
Professor Juha Töyräs, Ph.D.
University of Eastern Finland
Department of Applied Physics

Professor Jukka Jurvelin, Ph.D.
University of Eastern Finland
Department of Applied Physics

Adjunct Professor Simo Saarakkala, Ph.D.
University of Oulu
Department of Diagnostic Radiology

Reviewers:
Professor Kay Raum, Ph.D.
Charité - Universitätsmedizin Berlin
Julius Wolff Institut & Berlin-Brandenburg School for Regenerative Therapies
Berlin, Germany
email: Kay.Raum@charite.de

Koji Hattori, M.D., Ph.D.
Konan Women's University
Faculty of Nursing and Rehabilitation
Kobe, Hyogo, Japan
email: khattori@konan-wu.ac.jp

Opponent:
Directeur Pascal Laugier, Ph.D.
Universite Paris 6
Laboratoire d'Imagerie Parametrique CNRS
Paris, France
email: pascal.laugier@upmc.fr

ABSTRACT

Osteoarthritis (OA) is a progressive degenerative joint disease which causes pain, stiffness and abnormal remodeling of the joints. Currently, no healing cure exists for the disease, but with early diagnosis, the progression of the OA may be slowed down. Unfortunately, the earliest changes related to OA are not detectable with the current clinical imaging techniques. Furthermore, the development of surgical cartilage repairing techniques has created the need for novel quantitative techniques for evaluating of the integrity of articular cartilage and subchondral bone.

Quantitative ultrasound imaging is a sensitive technique for the detection of artificial degeneration of cartilage as well as the early signs of spontaneous osteoarthritis. Furthermore, with ultrasound, the integrity of spontaneously or surgically repaired cartilage can be evaluated. However, clinically applicable ultrasound imaging devices for arthroscopic evaluation of articular cartilage have not yet been introduced. In the present thesis, a novel arthroscopic ultrasound technique is introduced and evaluated. First, the technique was tested by imaging phantoms with variable surface characteristics and with mechanically or enzymatically damaged cartilage samples. Furthermore, the ability of the technique to evaluate the integrity of spontaneously healed and surgically repaired animal cartilage was investigated *in vitro* and the technique was compared with the optical coherence tomography (OCT), another high resolution imaging technique proposed for arthroscopic use. Finally, the clinical applicability of the proposed ultrasound technique was tested in arthroscopy of bovine knee joints *ex vivo* and human knee joints *in vivo*.

Ultrasound arthroscopy proved to be suitable for the detection of mechanical and enzymatical degeneration of articular cartilage. Furthermore, the integrity of spontaneously healed and surgically repaired cartilage could be determined with the technique. Significant correlations were detected between the ultrasound and OCT parameters. Mechanically degraded and spontaneously degener-

ated cartilage could be distinguished from intact cartilage by arthroscopic ultrasound evaluation of bovine (*ex vivo*) and human (*in vivo*) knee joints. Furthermore, the ultrasound evaluation of human knee articular cartilage provided important information on the integrity of the tissue not available from conventional arthroscopy.

The present results indicate that the ultrasound arthroscopy is a sensitive method for evaluation of the integrity of articular cartilage. Furthermore, ultrasound could provide valuable information on the integrity of repaired tissue. The introduced ultrasound technique was found to be suitable for arthroscopic use and to produce valuable diagnostic information. However, further technical development of the arthroscopic ultrasound catheters will be needed to enable more straightforward and reproducible clinical measurements.

Universal Decimal Classification: 534-8, 534.321.9
National Library of Medicine Classification: WE 300, WE 348, WN 208
Medical Subject Headings: Osteoarthritis/diagnosis; Diagnostic Imaging; Cartilage, Articular/ultrasonography; Ultrasonics; Arthroscopy; Tomography, Optical Coherence; Knee Joint
Yleinen suomalainen asiasanasto: nivelrikko - - diagnoosi; rusto; nivelet; kuvantaminen; ultraääni; ultraäänitutkimus

To Annika

Acknowledgements

This study was carried out during 2008-2011 at the Department of Applied Physics, University of Eastern Finland and Kuopio University Hospital.

First of all I would like to thank my supervisors for their encouragement and guidance during my thesis work. I am grateful to my principal supervisor professor Juha Töyräs for his never-ending enthusiasm, creativity and energy that I have been ruthlessly using during my Ph.D. project. I would like to thank my second supervisor professor Jukka Jurvelin for giving me an opportunity to work in his world-famous research group. I would also like to thank my third supervisor adjunct professor Simo Saarakkala, for sharing his knowledge on ultrasound and articular cartilage.

I am grateful to the official reviewers of this thesis, Koji Hattori, MD, Ph.D. and Professor Kay Raum, Ph.D., for their encouraging comments and constructive criticism. I also thank Ewen Macdonald, D.Pharm. for linguistic review.

I would like to express my deepest gratitude to all of my co-authors for their contributions.

It has been privilege to work with the cheerful, intelligent and unbelievably helpful people in the BBC-group. Especially, I would like to thank Erna Kaleva, Ph.D. and Heikki Nieminen, Ph.D. for introducing me to the world of ultrasound and articular cartilage, Katariina Kulmala, M.Sc. (Tech) and Antti Aula, Ph.D. for their irreplaceable help on practical issues, needed to get anything done in this fascinating world of science and bureaucracy, Lassi Rieppo, M.Sc. for helping with polarized light microscopy and Matti Timonen for programming custom-made softwares.

I would like to acknowledge the staff of the Institute of Biomedicine, Anatomy and BioMater Centre for their efforts on the sample preparation and all related issues. Furthermore, I would like to thank the staff of the Department of Applied Physics, especially,

Jarkko Leskinen, M.Sc. and Janne Heikkilä, Ph.D. for degassing PBS when ever needed.

I am grateful to my mother Raili and my sisters Anna, Elina and Liisa for their endless support and interest towards my doings during the Ph.D. project. I would also like to remember my father Markku Virén, who with his unique philosophy of life affected the lives of countless patients, colleagues and friends. He has been an inspiration and example for me through my whole live.

Finally, I owe my deepest gratitude to my "prettier half" Annika for her endless love and almost as endless understanding for the long working hours during my Ph.D. project. Without your support I might have quit the research for a long time ago.

For financial support Kuopio University Hospital (EVO grants 5041719, 5041716, 5041723 and 5041723), Päivikki and Sakari Sohlberg Foundation, Academy of Finland (projects 127198 and 128117), Sigrid Juselius Foundation, Jenny and Antti Wihuri Foundation, TBDP-graduate school and Instrumentarium foundation are acknowledged. Atria Lihakunta Oyj is acknowledged for providing the bovine joints as research material.

Kuopio, June, 2011
Tuomas Virén

ABBREVIATIONS

1D	one-dimensional
2D	two-dimensional
3D	three-dimensional
A-mode	1D amplitude representation of a reflected ultrasound wave
B-mode	2D ultrasound image
DD	digital densitometry
DMOADs	disease-modifying osteoarthritis drugs
FDA	Food and Drug Administration
FD-OCT	frequency domain optical coherence tomography
FH	femoral head
FMC	femoral medial condyle
FEPA	Federation of European Producers of Abrasives
FFT	fast Fourier transform
FIR	finite impulse response
GAG	glycosaminoglycan
ICRS	International Cartilage Repair Society
IVUS	intravascular ultrasound
LFC	lateral femoral condyle
LPG	lateral patello-femoral groove
MFC	medial femoral condyle
MR	magnetic resonance
MRI	magnetic resonance imaging
MTP	medial tibial plateau
NSAID	non-steroidal anti-inflammatory drugs
OA	osteoarthritis
OCT	optical coherence tomography
PAT	patella
PFG	patello-femoral groove
PLM	polarized light microscopy
PS-OCT	polarization sensitive optical coherence tomography
RF	radio frequency
RMS	root mean square
SEM	scanning electron microscopy
TD-OCT	time domain optical coherence tomography

SYMBOLS AND NOTATIONS

α_r	reflection coefficient
$R_c^{dB}(f)$	energy reflection coefficient
α_t	transmission coefficient
δf	frequency bandwidth
λ	wavelength
$\mu_c^{dB}(f)$	apparent backscattered energy
ν	Poisson's ratio
ϕ	angle between ultrasound transducer and cartilage surface
ρ	density
σ	cross-section
θ	angle between incident, reflected or refracted ultrasound wave and surface normal
$A_0(z, f)$	frequency and depth dependent attenuation function
A_i	amplitude of reflected ultrasound or optical signal
AIB	apparent integrated backscattering
b, m	medium dependent coefficients
b_i	mean value of optical signal recorded from cartilage inner structures
c	speed of sound
CV	coefficient of variation
d	distance between cartilage surface and imaging probe or distance between two measurement points
$diam.$	diameter
$E(f)$	acoustoelectric transfer function
E_{Dyn}	dynamic moduli
E_{Eq}	equilibrium modulus
f	ultrasound frequency
g	anisotropy coefficient
$G(f)$	acquisition system transfer function
$H^2(z, f)$	diffraction function
I	intensity
IRC	integrated reflection coefficient
k	wave number
m	number of scan lines
n	number of samples

OBS	optical backscattering
ORC	optical reflection coefficient
ORI	optical roughness index
p	pressure or p-value
r	radius
R	time domain reflection coefficient
$R_c\,(f)$	frequency dependent cartilage reflection coefficient
$R_r\,(f)$	frequency dependent reference reflection coefficient
S	area of ultrasound transducer
$S\,(z, f)$	frequency domain ultrasound signal
sCV	standardized coefficient of variation
TOF	time of flight
u_0	oscillation speed of ultrasound transducer
URI	ultrasound roughness index
Z	acoustic impedance
z	distance from ultrasound transducer
$\langle \dots \rangle$	spatial average

LIST OF ORIGINAL PUBLICATIONS

This thesis is based on the following articles referred to by their Roman numerals:

I Virén T, Saarakkala S, Kaleva E, Nieminen HJ, Jurvelin JS, Töyräs J: Minimally Invasive Ultrasound Method for Intra-Articular Diagnostics of Cartilage Degeneration, Ultrasound Med Biol, 2009 Sep; 35 (9): 1546-54.

II Virén T, Saarakkala S, Jurvelin JS, Pulkkinen HJ, Tiitu V, Valonen P, Kiviranta I, Lammi MJ, Töyräs J: Quantitative Evaluation of Spontaneously and Surgically Repaired Rabbit Articular Cartilage Using Intra-Articular Ultrasound Method *in situ*, Ultrasound Med Biol, 2010 May; 36 (5): 833-9.

III Virén T, Huang YP, Saarakkala S, Pulkkinen H, Tiitu V, Kiviranta I, Lammi MJ, Brunott A, Brommer H, van Weeren R, Brama PAJ, Linjama A, Zheng YP, Jurvelin JS, Töyräs J: Comparison of Ultrasound and Optical Coherence Tomography Techniques for Evaluation of Integrity of Spontaneously Repaired Horse Cartilage, Submitted to Phys Med Biol, 2011.

IV Virén T, Saarakkala S, Tiitu V, Puhakka J, Kiviranta I, Jurvelin JS, Töyräs J: Ultrasound Evaluation of the Mechanical Injury of Bovine Knee Articular Cartilage Under Arthroscopic Control, IEEE Trans Ultrason Ferroelectr Freq Control, 2011 Jan; 58 (1): 148-55.

V Kaleva E, Virén T, Saarakkala S, Sahlman J, Sirola J, Puhakka J, Paatela T, Kröger H, Kiviranta I, Jurvelin JS, Töyräs J: Arthroscopic Ultrasound Assessment of Articular Cartilage in Human Knee Joint: A Potential Diagnostic Method, Cartilage, in press 2010.

AUTHOR'S CONTRIBUTION

The publications selected to this dissertation are original research papers on arthroscopic ultrasound assessment of articular cartilage. The author has contributed on the development of the ultrasound measurement system and carried out all ultrasound measurements and signal analysis. The author has been the main writer in the studies I-IV.

Contents

1 Introduction

Articular cartilage is glass-like, smooth and white connective tissue covering the articular surfaces of long bones in diathrodial joints [109]. Articular cartilage is a primitive tissue without blood vessels and nerves [20,23,109]. Cartilage transmits, distributes and evens out the peak loads between the articulating bones [109]. Furthermore, cartilage enables almost frictionless sliding between articular surfaces [23,109]. In order to function properly cartilage has a complex structure and composition so it can display its unique anisotropic, and nonlinear mechanical properties, high durability and resistivity to wear [8,72,109]. Articular cartilage is composed of two phases: a fluid phase (70-80% of cartilage wet weight), composed of water and electrolytes, and a solid phase (the remaining 20-30%) composed of proteglycans, collagen fibrils, chondrocytes and glycoproteins [109]. Proteoglycans are responsible for the time-dependent and equilibrium properties of the tissue, whereas collagen fibrils are mainly responsible of tensile stiffness and the dynamic compressive properties of the cartilage [108].

Osteoarthritis (OA) is the most common musculoskeletal disease in the developed countries [5]. OA is a degenerative joint disease generally characterized by a progressive degeneration of the articular cartilage and remodeling and sclerosis of subchondral bone [20,23]. OA causes pain, stiffness, swelling, abnormal remodeling and limitation of the motion of the joints [20]. At the tissue level, OA causes degeneration of collagen network and loss of proteoglycans leading to an increase in the water content and a softening of the tissue [96,99,104]. The etiology of OA is still unknown but obesity, sex, genetic inheritance and cartilage injuries are known to be risk factors for the disease [20]. Although no healing cure currently exists for OA, the progression of the disease can be slowed down with the changes in lifestyle *e.g.* weight loss and changes in work conditions. Furthermore, the development of disease modify-

ing drugs for OA is under intense research [133]. However, the lack of quantitative techniques for clinical evaluation the outcome of the drug treatment has hindered the development of effective disease modifying agents [133].

Articular cartilage has a limited capability to undergo repair [23, 69, 109]. Thus, damage to articular cartilage can initiate the degeneration of the tissue and lead to the development of the post-traumatic osteoarthritis [15, 69]. In order to prevent the cartilage subsequent degeneration after injury variable surgical techniques such as microfracturing, autologous tissue transplantation and mosaicplasty have been proposed for repairing local cartilage injuries [17, 58, 148]. Unfortunately, the outcome of the surgery is often uncertain and dependent on the site and extent of the cartilage lesion and the age of the patient [18]. To enhance effectiveness of repair surgery quantitative techniques for delineation and classification of cartilage injuries are needed. Furthermore, better techniques for monitoring the healing of the cartilage and for evaluation of the outcome of repair surgery are essential for the development of novel surgical techniques [18, 69].

Currently, X-ray imaging, magnetic resonance imaging (MRI) and arthroscopy are used for evaluating the severity of cartilage injuries. Unfortunately, these techniques are not accurate enough for assessing the extent of cartilage damage, the integrity of adjacent tissue and performance of cartilage repair tissue. Cartilage is not visible in X-ray images due to the similar attenuation in the surrounding soft tissues. Currently, the only clear changes in subchondral bone and joint space narrowing related to wear of the articular cartilage can be detected in clinical X-ray images. Poor resolution of clinical MRI can lead to misdetection or underestimation of the extent of injured tissue volume [18]. Arthroscopy enables visual evaluation and mechanical probing of the articular cartilage. However, arthroscopy is a subjective investigation and highly dependent on the experience of the operating surgeon. Furthermore, in a recent study, the majority of experienced athroscopisists found it difficult to discern between high and low grade cartilage damage and

considered that some device that could provide a quantitative measurement of the integrity of the articular cartilage would be useful or very useful [147].

Ultrasound is potetially useful method for evaluating the integrity of articular cartilage. With ultrasound, the degeneration of collagen network [29, 61, 138, 142], the roughness of cartilage surface [2, 28, 138] and variation in cartilage thickness [29, 68, 142] can be sensitively detected. Furthermore, the size and severity of local cartilage injuries and the integrity of cartilage repair can be evaluated with ultrasound [35,49,64,90]. Ultrasound measurements have already been conducted during open knee surgery and arthroscopy *in vivo* [62, 63]. However, a quantitative ultrasound system capable of performing ultrasound imaging could be more suitable for clinical use than the point measurements. Currently no quantitative ultrasound imaging devices suited for arthroscopic use have been introduced.

Intravascular ultrasound is a clinical high frequency imaging modality originally designed for the imaging of vascular walls [120]. An IVUS instrumentation consists of an ultrasound catheter (*diam.* = 1 mm) incorporating a miniaturized ultrasound probe and a main unit containing signal and image processing circuits. With the IVUS technique, the area of the artery lumen as well as amount and composition of plaque can be approximated inside the arteries [120]. The IVUS technique is used to detect and measure the size of atheromas and can help in the selection of the proper intervention strategy [120]. The technique can deliver a real time high resolution image. Furthermore, because the ultrasound catheter is thin, flexible and sterile, the IVUS technique could be feasible also for arthroscopic use.

Optical coherence tomography (OCT) is a relatively new technique for imaging of articular cartilage. OCT is based on the measurement of light reflected and backscattered from cartilage surface and inner structures [32, 33, 57, 164]. With OCT, the orientation of collagen fibrils and typical OA related changes can be estimated. Furthermore, the cartilage surface reflection [57, 141], sur-

face roughness [141], and organization and disorganization of the collagen network can be quantified with OCT [164]. Importantly, OCT has already been used during open knee surgery and in arthroscopy [33].

In this thesis work, a novel arthroscopic ultrasound technique for imaging of articular cartilage will be introduced. The suitability of the technique for detecting the artificial OA related changes in articular cartilage as well as evaluation of the integrity of spontaneously healed and surgically repaired articular cartilage has been systematically investigated. Furthermore, the technique was compared with optical coherence tomography, another high resolution imaging technique proposed for arthroscopic use. In an atempt to develop the technique towards clinical use, it has been tested in experimental arthroscopies of bovine knee joints *ex vivo*. Finally, the clinical potential of the technique was tested in routine arthroscopies of patients suffering from various degenerative conditions of the knee joint *in vivo*.

2 Articular cartilage

Articular cartilage is a primitive connective tissue which has no nerves or blood vessels [109]. In order to function correctly, cartilage has a non-homogenous composition as well as a complex and highly organized structure which give cartilage its unique mechanical properties and high durability [109]. If the composition or structure of articular cartilage is disturbed, the mechanical properties and durability of the cartilage may change which can lead to degeneration of the tissue [20, 109]. Unfortunately, cartilage has very limited resources to repair itself and cartilage damage is usually irreversible [69]. In this chapter, the structure and composition of the articular cartilage, the development and progress of osteoarthritis, and clinical and pre-clinical methods to diagnose and repair damaged cartilage will be briefly reviewed.

2.1 STRUCTURE AND COMPOSITION

Articular cartilage is white, class-like hyaline cartilage [109]. Hyaline cartilage has an unhomogenous highly organized structure composed of extracellular fluid, solid matrix and cells [109]. The extracellular fluid is composed of water and electrolytes. Cells are embedded in a solid matrix which is mainly composed of collagen fibrils, proteoglycans and glycoproteins [109].

Interstitial fluid contributes 60% - 80% of cartilage total weight and is composed of water and electrolytes [109]. The interstitial fluid makes a major contribution to the mechanical behavior of the articular cartilage [109] and it confers lubrication for the articular surfaces and provides the nutrition for the chondrocytes [72, 109]. In healthy cartilage, the water content decreases towards the deep zone of the cartilage [109].

Collagen fibrils are proteins which mainly consist of type II collagen [109]. The collagen fibrils account for 10% - 20% of the car-

tilage wet weight. The type II collagen consists 90% - 95% of all cartilage collagen [23]. The collagen content decreases from surface to the middle zone and increases again in the deep zone [155]. Collagen fibers exist in a highly organized network within the cartilage matrix. At the cartilage surface, the collagen fibers are orientated in parallel to the articular surface. In the middle zone the collagen orientation is random although a slight preference for the 45° orientation to the articular surface can be detected [7]. In the deep zone, collagen orientation changes to being perpendicular to the cartilage surface. In addition to type II, at least type IX and XI collagen can be found in articular cartilage. The function of these collagens is not fully understood but it is believed that they stabilize the collagen meshwork and connect the collagen fibrils with proteoglycan molecules [23, 109].

Proteoglycans are glycoproteins which are connected to the hyaluronan chains. Proteoglycans are composed of glycosaminoglycan (GAG) proteins which are connected to the core protein [109]. A proteoglycan aggregate is formed when the proteoglycan monomers are bound to a hyaluronate monofilament chain [109]. Proteoglycans account for 4% - 7% of cartilage wet weight [109]. Proteoglycans form the solid matrix inside the cartilage together with collagen fibrils. The proteoglycan concentration is lowest at the superficial cartilage and increases towards the deeper layers [109]. GAG proteins are negatively charged which causes osmotic swelling pressure inside the cartilage. The collagen network resists the swelling pressure, giving cartilage its shape [99].

Chondrocytes form 1% - 7% of cartilage wet weight [109]. The number, shape and distribution of the cells vary between different depths in cartilage. On the cartilage surface, the cells are elliptical and the number of cells is high. Deeper in the tissue the number of cells declines and the shapes of the cells become more spherical. Near the cartilage subchondral bone interface number of chondrocytes again increases. In this area, the chondrocytes are spherical and organized in columns.

Articular cartilage can be divided into four sections according

to its structural properties: superficial tangential zone, transitional zone, deep zone and calcified cartilage (Figure 2.1) [51,113].

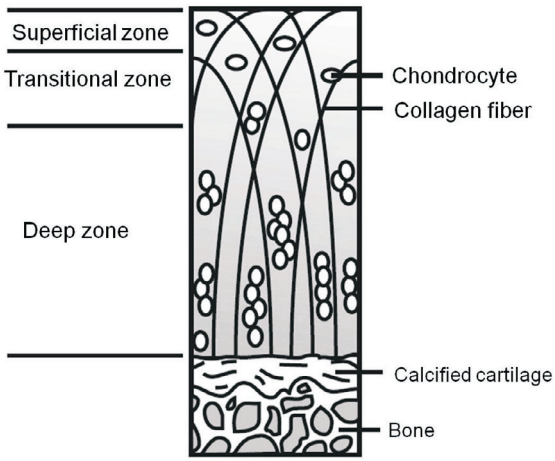

Figure 2.1: Cartilage structure can be divided into four zones: Superficial tangential zone, transitional zone, deep zone and calcified cartilage [113].

2.2 FUNCTION

The primary function of the articular cartilage is to transmit and even out the peak loads between articulating bones and contribute to the joint lubrication [109]. The interaction between interstitial water, the collagen fiber network and proteoglycans determines the mechanical properties of cartilage [109]. In highly dynamic compression, the water has no time to flow out from the cartilage and a high pressure is created within the cartilage [109]. The collagen network resists the deformation caused by the elevated hydrostatic pressure and therefore cartilage is very stiff under dynamic loading. In an intact joint, pressurized water bears 95% of the load protecting the solid matrix from high loads [109]. Under static compression, cartilage interstitial water starts to flow out and cartilage deforms [109]. Fluid flow contributes to the time-dependent viscoelastic properties of the cartilage. In a static compression, water flows out of cartilage until equilibrium is reached between the

repulsion force of the negatively charged proteoglycans and compressing force [109]. The Collagen network is known to be more responsible for the dynamic and tensile response of cartilage whereas proteoglycans are responsible for time-dependent and equilibrium responses of cartilage [85, 109, 137].

Cartilage enables almost frictionless sliding between the articular surfaces. According to current knowledge, at least two lubrication mechanisms are present at the articulating surface [8, 72]. In dynamic loading the interstitial water pressure bears loads and lubricates the joint [8]. In static loading the synovial fluid and its proteins are reponsible for lubricating the joint according to the boundary lubrication theory [72]. Furthermore, the lubricin present at the cartilage surface has also been proposed to contribute the wear resistance of articular cartilage [72]

2.3 OSTEOARTHRITIS

Osteoarthritis (OA) is the most common joint disorder in the world [5]. Radiographic evidence of OA can be detected from 80% of individuals over 75 years of age [5]. In some populations, 75% people over 65 have OA in one or more joints [45]. OA not only decreases the quality of the life of the patient but it is also responsible for a significant burden to society. OA is the second most common cause of work disability of men over 50 years in the USA accounting for significant direct and undirect costs to society [5]. Annually, OA costs approximately 60 billion dollars in the United States alone [39]. Since age is the greatest risk factor for the disease, the aging of population will further increase the significance of OA in the future.

The clinical symptoms of OA are pain, stiffness and swelling of the joints [20]. At the tissue level, OA causes degeneration of the articular cartilage and sclerosis and abnormal remodeling of the subchondral bone [20]. OA can affect any synovial joint but, is most commonly found in the joints of hand, foot, knee, spine and hip [22]. Although, the initial cause of the OA is usually un-

known many risk factors have been identified [22]. Age is the most important risk factor of OA [39]. Being overweight [41, 43], joint injuries [15, 100, 160], abnormal anatomy [44, 60], genetics [94] and muscular weakness [146] are also significant risk factors for the development of OA. Traditionally OA has been classified into two categories: primary and secondary OA. When the disease develops without any known reason it is called the primary OA. In secondary OA the initial cause of the degeneration of the tissue is known. Secondary OA can be classified into metabolic, anatomic, traumatic and inflammatory OA according to the initial cause of the degeneration [20]. Unfortunately, no healing cure exists for OA and the current treatment of the disease is focused on pain relief and treatment of the inflammation [20, 22].

2.3.1 Development and progress

The development of the OA is usually slow, taking several years even decades. The first sign of the OA is the disruption of the solid matrix [20, 109]. The disruption of the solid matrix can be due to mechanical injury, a metabolic disorder or inflammation [20]. Disruption of collagen network with a simultaneous decrease in the proteoglycan content accompany the increase in cartilage water content and swelling of the tissue [20,98,99]. These changes increase the permeability of the cartilage, the tissue becomes softer and more vulnerable to further damage, *e.g.*, due to mechanical overloading [6, 20].

When the chondrocytes detect cartilage damage by changes in the osmolarity, charge density or strain, the repair response starts [20]. The repair response can last for years and the progression of the disease can be even temporarily interrupted. At this stage, it is known that medical interventions *e.g.* the alteration of the joint loading can promote the repair response and stimulate the restoration of the cartilage [19, 122, 161]. The repair response including synthesis of solid matrix proteins and cell proliferation may stabilize or restore the articular cartilage [20].

The failure of the repair response leads to the degeneration of the cartilage and development of OA. The damaging of the collagen network causes the fibrillation of the cartilage surface and the formation of deep fissures, even holes in the cartilage [20]. The decrease in cartilage stiffness is responsible for to increased loading of subchondral bone. This can lead to sclerosis, formation of cysts and abnormal remodeling of the subchondral bone [21]. Further degeneration of the articular cartilage leaves bare subchondral plates articulating with each other [20]. At this stage, the mobility of joint is restricted or lost and the only treatment option is total joint replacement surgery.

Subchondral bone is known to have a significant role in the development of OA. It has been proposed that the stiffening of subchondral bone might even initiate the degeneration in OA [134]. Radin *et al*. have proposed that the stiffening of subcondral bone increases the loading of the articular cartilage which triggers cartilage degeneration [134]. Currently, it is still unclear exactly what factor or factors initially causes OA. However, it is clear that, the evaluation of the integrity of both articular cartilage and subchondral bone could be crucial for the early detection of OA.

2.3.2 Treatment and prevention

Currently no healing cure exists for OA and the treatment is mainly focused on relieving pain and maintenance of function and mobility of the patient. The current treatment of OA usually consists of anti-inflammatory drugs, rehabilitation, physiotherapy, loss of weight, undertaking strength and range of motion exercises and raising awareness in the patient [145]. In the late stage of OA, total joint replacement can be offered as a treatment [80]. It has been reported that approximately 90% of the patients achieve pain relief and an improvement in joint function following total hip or knee replacement [80]. However, the high cost of the surgery and revisions of the surgery due to the failure of the prostatics dearly limit the use of total joint replacement for the treatment of OA [80].

The prevention of OA is focused on minimizing the known risk factors related to the development of OA. The most important modifiable risk factors of OA are obesity, joint injuries, and abnormal loading of the joint. It has been estimated that a reduction of obesity, prevention of joint injuries and modifying the joint loading, *i.e.*, changes in work conditions might prevent over half of new OA cases [42]. Furthermore, with variable surgical techniques, it might be possible to restore the cartilage surfaces and prevent the development of OA after joint injury [11,69].

Pharmaceutics

Currently, the pharmacological treatment of OA consists of symptom-modifying treatments such as analgesics, non-steroidal anti-inflammatory drugs (NSAIDs) and intra-articular injections of hyaluronic acid or glucocorticoids [50]. NSAIDs are usually effective in the early and middle stages of the disease but they are inadequate for pain relief in the late stages of OA [50]. Furthermore, the gastrointestinal and cardiovascular side effects such as gastric and intestinal inflammation and heart attacks have limited their use [13,50].

Inra-articular injections of hyaluronan or glucocorticoids are used for pain relief. Since the injection is given directly into the arthritic joint, severe systemic side effects are avoided [50]. With intra-articular injections, pain relief for up to 6 months can be achieved with fewer side effects than with the use of NSAIDs [50]. Furthermore, hyaluronan injections might have some disease-modifying potential, at least in the early stage of the disease [55]. However, the efficiency of the disease-modifying effect of the intra-articular injection may be only slightly better than that of the placebo treatments [50,92]

In an attempt to terminate the degeneration of cartilage and restore the tissue, disease-modifying drugs (DMOADs) are under intense research [133]. DMOADs are intended to prevent, retard, stabilize or reverse the degenerative changes related to OA [129]. Sev-

eral drugs have been proposed for inhibition of matrix metalloproteinase response [25] or modulation of subchondral bone turnover [79]. However, no disease modifying effect of these drugs has been demonstrated in the clinical studies so far. Nevertheless, DMOADs are under intense research and novel promising molecules are already undergoing pre-clinical or clinical testing [133].

Surgical techniques

When the pharmacological treatments fail to relieve the pain and restore the function of the joint, the surgical interventions may be considered. Most commonly, cartilage surgery is used to repair local cartilage injuries usually caused by high impact loading. Operative treatments include alteration of joint alignment, debridement, microfracturing, whole tissue transplantation and autologous chondrocyte transplantation [11]. In the following sectioin, these surgical techniques will be briefly reviewed.

Alteration of joint alignment is used to ease the symptoms of local cartilage injury. The alignment of the joint is modified to minimize the loading on the injured cartilage and to transform the loading to intact tissue. Joint alignment can be altered by using a muscle release technique, or osteotomy [19]. In the muscle release technique the muscles acting across the joint are sectioned to alter the joint loading as muscles contract [19]. In osteotomy, the articular surfaces are realigned in attempt to decrease loading on most severely damaged cartilage areas [19]. Osteotomy may also be used to correct malalignment that can contribute to the degeneration of articular cartilage. In clinical studies, significant pain relief, increase in joint mobility and increase in radiographic joint space have been reported directly after muscle release surgery or osteotomy [1, 102, 135, 143]. However, these techniques are not widely used because of the uncertain outcome of the operation and the decline in the clinical results over time [70, 161]. Debridement is used to remove the loose fragments of cartilage or meniscus and to smooth the fibrillated cartilage surfaces [124]. Removal of these

loose fragments from the joint improves the functions but no clinical evidence has been reported for debridement to actually modify the progression of the OA [19]. Furthermore, the shaving of cartilage surfaces may even accelerate the degeneration of the tissue [81].

Bone marrow stimulation *i.e.* microfracturing, is the most frequently used operative technique for treatment of small cartilage injuries in the knee joint [11]. Microfracturing is a relatively inexpensive and technically straightforward cartilage repair technique. In microfracturing, the injured cartilage and the underlying calcified cartilage are removed to create a well shouldered cartilage lesion extending to the subchondral bone [16, 107]. Perforation of the exposed subchondral bone allows the formation of the blood clot in the cartilage lesions. The lesion is populated by the mesenchymal stem cells leaking from the bone marrow [16]. Subsequently, the stem cells differentiate into fibrous chondrocytes and fibrocartilaginous repair tissue is formed around the injury, creating a new cartilage surface [11]. Although good, even excellent, results have been reported after treatment of small cartilage lesions with microfracturing, the outcome of the surgery is still uncertain [11]. Patient selection is critical for good clinical results. Better surgical outcomes have been reported in young and normal weight patients [87, 106, 107]. Furthermore, the clinical results seem to deteriorate over time [105, 107].

Transplantation techniques provide an efficient way to resurface osteochondral defects of the knee [11]. These techniques involve transplantation of osteochondral plugs to the defected cartilage area to create new hyaluronan cartilage [58, 167]. The osteochondral transplants can be harvested from the low weight bearing areas of the patients (autologous osteochondral transplantation) joint [58] or from a cadaver donor (osteochondral allograft transplantation) [167].

In autologous osteochondral transplantation, small cylindrical ostochondral plugs are harvested from the low weight bearing areas of the joint and transplanted into the defected area [58]. The advantage of the technique is that the procedure can be conducted

during a single operation and the cartilage defect is filled with viable hyaline cartilage extracted from the same individual. The outcomes of the autologous mosaicplasty treatments of symptomatic chondral defects have been encouraging. Various studies have reported good or excellent results after repair of cartilage defects [58, 125, 126]. However, because of the limited number of possible donor sites, only patients with small symptomatic cartilage defects can be treated with this technique. Furthermore, the healing of the donor site, the integration of the osteochondral transplant into the adjacent tissue and the difference in the thickness, composition and structure of the donor and adjacent cartilage diminish the efficiency of the technique [11, 83, 84].

In order to transplant similar cartilage as the adjacent tissue and to minimize the dead space between the transplant and adjacent tissue, osteochondral allograft transplantation has been proposed for the repair of cartilage defects [167]. In osteochondral allograft transplantation, cartilage with viable chondrocytes and intact subchondral bone is transplanted from a cadaver onto the cartilage defect [167]. The advantage of this technique is that the transplant can be harvested from the same site as the repair site [11]. Furthermore, the dead space between the adjacent cartilage and transplant can be minimized by matching the shape and size of the transplant to the cartilage defect [11, 167]. The viability of chondrocytes is crucial for successful transplantation and, thus, fresh allografts are usually utilized [11]. Cryopreserved or fresh frozen allografts enable longer storage times, decrease the disease transmission risk and reduce immunogenicity [11, 40]. However, cryopreserving and freezing can lead to lower chondrocyte viability and initiation of degenerative changes in the allografts [11]. Good or excellent outcomes have been reported in various clinical studies in which allografts have been used to repair unipolar cartilage defects [24, 31, 52, 103, 144]. However, the outcome of the procedure is uncertain in cases of bipolar defects and primary OA including inflammatory changes [24, 34]. Furthermore, immunogenicity and the risk of transmission of diseases have limited the use of the os-

teochondral allograft transplantation technique [11].

Autologous chondrocyte transplantation is an innovative technique for restoring the cartilage surfaces. The technique involves a minimum of two operations in which the chondrocytes are first harvested from low weight bearing areas of the joint and in the second operation, the chondrocytes are implanted into the cartilage injury covered with a periosteal graft [17]. In the best case scenario, the repair leads to regeneration of hyaline like cartilage [17]. Good or excellent results have been reported after treatment of cartilage injuries with autologous chondrocyte implantation [17,168]. Furthermore, the technique has been reported to be more efficient than the microfracturing or osteochondral transplantation techniques [12]. However, the operation does require a minimum of two surgical operations and a long rehabilitation period [11]. Furthermore, complications related to the harvesting of the periosteal grafts have been reported [53,82].

2.3.3 Diagnostic methods

Clinical methods

Currently, OA is diagnosed by clinical examination, *i.e.*, anamnesis, investigation of the range of motion and palpation of the joints. X-ray imaging and magnetic resonance imaging (MRI) are often used clinically to confirm the diagnosis of OA. From an X-ray image the OA related abnormal remodeling of the subchondral bone and narrowing of the joint space related to the wear of articular cartilage can be diagnosed. However, because the similar attenuation of X-rays in the surrounding tissues, cartilage is not directly visible in the X-ray images. Because of this, only the advanced changes related to OA can be radiographically detected.

MRI is a very promising non-invasive clinical imaging method for the diagnostics of OA. With MRI, the thickness of the articular cartilage, size and severity of the cartilage lesions and OA related changes in the subchondral bone, ligaments and meniscus can be detected [38]. However, the poor resolution of current clinical MRI

devices, their high costs and poor availability have limited the use of MRI in the diagnostics of OA and cartilage injuries. In addition to qualitative examination of the MRI images, quantitative MR parameters have been introduced for evaluating of the integrity of articular cartilage. It has been proposed that T_2 relaxation time would be related to the integrity of the collagen fibril network [37, 118]. Furthermore, the T_1 relaxation time in the presence of a gadolinium contrast agent has been shown to be related to the amount of proteoglycan in the cartilage [9, 10]. However, the quantitative MR-parameters are currently used mainly in pre-clinical and *in vitro* studies.

Arthroscopy is the standard procedure utilized to evaluate the size and severity of a cartilage injury. In some cases, arthroscopy is used also to evaluate the stage of OA. Arthroscopy enables visual evaluation and mechanical probing of the cartilage surfaces. Cartilage scoring systems have been introduced, *e.g.*, International Cartilage Repair Society's (ICRS) scoring to classify the cartilage injuries [18]. In order to grade the cartilage injuries, the operating surgeon approximates the depth of the lesion relative to the cartilage thickness, the integrity of the cartilage surface and the stiffness of the cartilage tissue [18]. According to the ICRS scoring, cartilage integrity can be divided into 5 categories (grades 0-4): intact (grade 0), nearly normal (grade 1), abnormal (grade 2), severely abnormal (grade 3-4). Unfortunately, arthroscopy is a subjective investigation and significantly dependent on the experience of the operating surgeon. In the study of Oakley et al. in which plastic knee models were investigated under arthroscopy, only a poor correlation was found between the true size of the lesion drawn on a plastic knee and the evaluation of severity made by the surgeons [121]. In a recent study, the majority of experienced arthroscopists found it difficult to discern low- and high-grade cartilage damage and consider the current diagnostic tools as being inadequate [147]. Furthermore, 75% of the arthroscopists consider that the use of any quantitative instrument during an arthroscopy would be very useful or somewhat useful for diagnostics [147].

Pre-clinical methods

novel quantitative methods are needed to detect the early changes related to the OA and sensitively evaluate the severity and extent of the cartilage injuries. Various techniques have been proposed for estimating the integrity of articular cartilage.

Mechanical indentation techniques have been used to quantify the mechanical competence of articular cartilage [4, 93]. With mechanical indentation techniques, the stiffness of the cartilage can be quantitatively measured during arthroscopy [93]. Since the cartilage thickness has an effect on the measured cartilage stiffness [65] an ultrasound indentation technique has been developed for quantitative measurements of cartilage stiffness [89, 140]. In ultrasound indentation, the cartilage thickness is measured with the ultrasound transducer used as an indenter. When the ultrasound transducer is pressed against the cartilage surface, the stress and strain can be measured with strain gauges and with ultrasound, respectively [89].

Optical coherence tomography (OCT) is a relatively new technique for cartilage imaging. In principle, OCT is analogous with ultrasound with the exception that near infrared light is used instead of sound waves. OCT is based on the measurement of the light being reflected and scattered from cartilage surface and inner structures [32, 33, 57, 164]. With OCT, cartilage thickness, surface roughness and reflection can be quantitatively evaluated [57, 141, 164]. Furthermore, with polarization sensitive OCT, the alignment and organization / disorganization of the collagen fiber network can be evaluated [164]. OCT has already been applied during clinical open knee surgery and arthroscopy [33]. The advantage of OCT is its superior resolution *e.g.* when compared with ultrasound or MRI. However, due to the extensive attenuation of light in biological tissues, the penetration of the light is limited to less than 2 mm which effectively limits the measurements of the cartilage thickness and prevents the imaging of subchondral bone [57].

Quantitative ultrasound techniques are potential methods for

assessing the integrity of articular cartilage and subchondral bone. With ultrasound one can evaluate cartilage thickness [110,142], surface reflection [29,77,138,142,154], surface roughness [2,78,138,139], integrity of cartilage collagen network [30,49] and integrity of subchondral bone [139]. Ultrasound has also been used to estimate the integrity of cartilage repair [49,90]. However, all of these studies have been conducted with laboratory instruments not suitable for clinical use. Clinical non-invasive ultrasound devices have been used to evaluate the integrity of articular cartilage, the extent of cartilage lesions and the integrity of subchondral bone [91,101,111]. However, the usability of non-invasive ultrasound measurements is limited because of shadowing due to the bones surrounding joint capsules and the disturbing effects of the soft tissues overlying the cartilage. In on attempt to avoid these limitations, ultrasound measurements have also been conducted during open knee surgery and arthroscopy [62, 63]. In arthroscopic conditions, all cartilage surfaces may be investigated. However, the invasiveness of this investigation may limit the usability of the arthroscopic ultrasound techniques.

3 Ultrasound

Ultrasound is a mechanical wave motion with a frequency that exceeds the human hearing range (*i.e.* over 20 kHz). Ultrasound waves can propagate through a medium in various different wavemodes. The medical imaging applications are usually based on the use of the longitudinal wavemode. In the longitudinal wave mode, the particles are oscillating in the same direction as the wave is propagating [162]. The transverse wave occurs when the particles are oscillating perpendicularly to the direction of wave propagation. Generally, transverse waves can exist only in solid materials. In fluids with no shear elasticity only longitudinal waves are supported. Other waveforms such as surface waves (combination of longitudinal and transverse waves) also do exist, but they have only a minor application in medical imaging [162].

3.1 ULTRASOUND AND MATTER INTERACTIONS

When an ultrasound wave propagates in a medium the particles within the medium are individually forced to oscillate. To simplify the mathematical description of sound propagation, the medium is often modeled as being homogenous, isotropic and elastic [162]. If these assumptions are valid, then the speed, reflection, refraction, attenuation and scattering of an ultrasound wave can be characterized with the equations presented in this chapter.

The speed of ultrasound wave is defined as the product of the wavelength (λ) and frequency f (Table (3.1), Equation (3.1)) [36]. The speed of ultrasound is dependent on the density and elasticity of the medium [162]. It can be shown that the speed of ultrasound depends on Young's modulus Y, Poisson's ratio ν and density ρ (Equation (3.2)) [162]. As the values of the density and elastic parameters (Equation (3.2)) are temperature dependent, the speed of ultrasound will vary as a function of the medium temperature [162].

Characteristic acoustic impedance is a material property defined by density ρ and speed of ultrasound c in the medium (Equation (3.3)) [162]. At the interface of two materials, the difference in the characteristic impedances defines the amplitude of reflection [36, 162]. Sound intensity I is defined as the ultrasound energy propagating through an unit area in an unit time. The intensity can be determined if the pressure amplitude p of the ultrasound wave and the characteristic impedance Z of the medium are known (Equation (3.4)) [36].

When the ultrasound wave propagates through an interface of two acoustically different materials, part of the wave is reflected from the interface. The angles of reflected θ_r and refracted θ_t waves can be determined by applying Snell's law (Equation (3.5)).

By assuming specular reflection (no scattering) the proportions of transmitted and reflected waveforms can be quantified by determining the intensity reflection α_r and transmission coefficients α_t (Equations (3.6) and (3.7)) [162]. If the interface between materials 1 and 2 is not ideal, but is irregular or rough, scattering in addition to the specular reflection occurs. The analytical solution for reflection and scattering from a rough irregular interface is very complicated and modeling is often applied.

When a sound wave propagates in a non-ideal material the ultrasound attenuates. Several processes are involved in the attenuation *e.g.* absorption and scattering. In absorption, the viscotic properties of the medium transform the energy of ultrasound wave into heat. In scattering, part of the initial sound field energy is scattered from the discontinuation points within the medium [36, 162]. The attenuation is exponentially related with the propagated distance (Equation (3.9)) and it is dependent on the frequency f (Equation (3.10)) [36, 162]

If the medium in which the ultrasound wave is propagating is not homogenous, the sound wave is scattered from the discontinuity points within the medium. The scattering involves both reflection and refraction phenomena [36]. The scattering is described by the scattering cross-section σ. The scattering cross-section expresses

the probability of the interaction between ultrasound wave and the scatterer. The cross-section is defined as the fraction of the intensity of scattered ultrasound and the intensity of the initial sound wave [36]. In the case of spherical scatterers, the cross-section is related to the wavenumber k and the radius of the scatterer r (Equation 3.8). Depending on the cross-section, the scattering events can be divided into three categories [36]. When the scatterer is small compared to the wavelength, the ultrasound is scattered uniformly in all directions. If the scatterer is large compared with the wavelength, the scattering will follow Snell's law. When the wavelength is of the same magnitude with the scatterer, then the shape of scattered field is complex being dependent on the size, shape and characteristic impedance of the scatterer [71,162].

All of the above mentioned scattering phenomena are present when ultrasound propagates in biological tissues. For example, specular reflection according to Snell's law and scattering can occur at the boundaries between large organs whereas uniform scattering takes place when ultrasound propagates through a blood vessel containing red blood cells ($diam.$ = 6-8 μm) [36].

3.2 GENERATION OF ULTRASOUND

In medical applications, ultrasound is usually created by transforming electrical signal into mechanical vibration by using piezoelectric crystals [36]. A piezoelectric material changes its physical dimensions as electrical voltage is applied between its faces [36,162]. This phenomenon is called the piezoelectric effect. The piezoelectric effect is of an inverse nature *i.e.* when mechanical pressure makes the piezomaterial oscillate, an oscillating electrical pulse can be measured between the faces of the crystal [36,162].

A simplified cross-section of an ultrasound transducer is presented in the Figure 3.1. An ultrasound transducer consists of a piezoelectric crystal, a case, a backing material and a matching layer. For optimal functioning of the transducer, the thicknesses and characteristic impedances of the backing material, matching layer

Table 3.1: Basic equations describing propagation of ultrasound wave in an elastic, isotropic and homogenous material.

Parameter	Equation	Number
Phase velocity	$c = f\lambda$	(3.1)
Speed of ultrasound	$c = \sqrt{\frac{Y(1-\nu)}{(1-2\nu)(1+\nu)\rho}}$	(3.2)
Characteristic impedance	$Z = \rho c$	(3.3)
Intensity	$I = \frac{p^2}{2Z}$	(3.4)
Snell's law	$\frac{\sin\theta_i}{\sin\theta_t} = \frac{c_1}{c_2}$	(3.5)
Reflection coefficient	$\alpha_r = \left(\frac{Z_2\cos\theta_i - Z_1\cos\theta_t}{Z_2\cos\theta_i + Z_1\cos\theta_t}\right)^2$	(3.6)
Refraction coefficient	$\alpha_t = \frac{4Z_2Z_1\cos^2\theta_i}{(Z_2\cos\theta_i + Z_1\cos\theta_t)^2}$	(3.7)
Scattering cross-section	$\sigma = k^4r^6$	(3.8)
Attenuation law	$p(z) = p_0e^{-\alpha z}$	(3.9)
Attenuation coefficient	$\alpha = bf^m$	(3.10)

f = ultrasound frequency
Y = Young's modulus
ν = Poisson's ratio
ρ = density
p = pressure amplitude
Z = characteristic impedance
c = phase velocity
p_0 = inital pressure amplitude
z = depth
α = attenuation coefficient
b = medium dependent coefficient
m = medium dependent coefficient
r = radius of a scatterer
θ = angle between ultrasound beam and surface normal
k = wavenumber

and piezoelectric crystal must be optimized. For optimal transmission of the ultrasound from the transducer to the imaged medium one or several matching layers are added between the ultrasound transducer and the medium to be imaged. With the matching layer the characteristic impedance of the piezoelectic crystal is matched with that of the medium to minimize the reflections at the inter-

face between the crystal and the medium [36]. The thickness of the matching layer is usually selected to be one fourth of the ultrasound wavelength [36]. Then the ultrasound reflected from the interface between matching layer and medium are in the same phase with the wave transmitted from the crystal as it reflects from the interface between the matching layer and the ultrasound crystal [36]. In ultrasound imaging, one requires short ultrasound pulses in order to achieve good axial resolution [36]. Since the piezoelectric crystal is transmitting waves in both the forward and backward directions, if one wishes to obtain short ultrasound pulses the material behind the crystal must absorb ultrasound effectively [36].

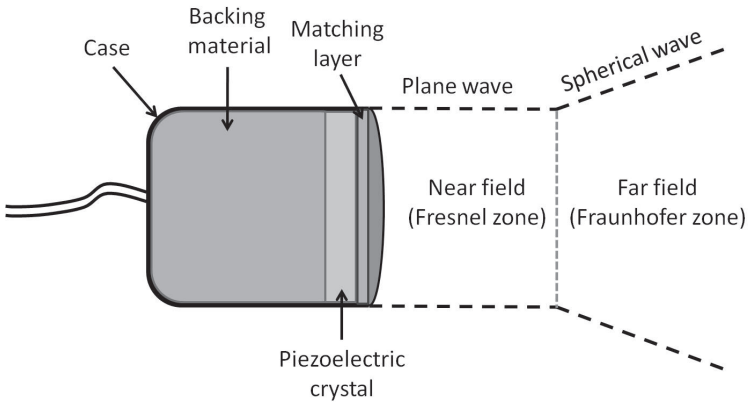

Figure 3.1: A simplified cross-section of a non-focused ultrasound transducer. The ultrasound field transmitted from a non-focused transducer can be divided into two sections: The near field where ultrasound wave propagates as a plane wave and the far field where ultrasound wave propagates as a spherical wave.

3.2.1 Non-focused ultrasound transducers

The function of a simplified non-focused ultrasound transducer can be modeled as a mechanical piston (radius = r), which is oscillating in the normal direction with respect to its surface transmitting continuous sine wave at a desired frequency. The ultrasound field transmitted from a non-focused ultrasound transducer can be divided into two zones. The ultrasound field near to the transducer

is called as the Fresnel zone or the near field [36]. In the Fresnel zone, the ultrasound wave propagates as a plane wave and the pressure of the ultrasound field changes rapidly as a function of the distance z from the transducer (figure 3.1) [36]. Mathematically in this model the pressure of an ultrasound field as a function of distance can be determined as follows

$$p(z) = \rho_0 c u_0 \left| \sin \left\{ \frac{kz}{2} \left[\sqrt{1 + \left(\frac{r}{z} \right)} - 1 \right] \right\} \right|, \tag{3.11}$$

where the ρ is density of the media, u_0 is the oscillation speed of the piezoelectric crystal, c is the speed of sound in the medium and k is the wave number. The location of the pressure maxima and minima can be calculated as follows (3.11)

$$\frac{kz}{2} \left[\sqrt{1 + \left(\frac{r}{z} \right)} - 1 \right] = \frac{m\pi}{2}, \tag{3.12}$$

where the uneven and even values of m correspond to the intensity maxima and minima of the ultrasound field, respectively. The last intensity maximum is achieved when m=1. This point is called as the last axial maximum and it is the boundary between the Fresnel and Fraunhofer zones [36]. Assuming that the distance z from the transducer is significantly greater than the radius (r) of the ultrasound probe ($r << z$), then the location (z_{lam}) of the last axial maximum can be determined as follows 3.12

$$z_{lam} = \frac{r^2}{\lambda}. \tag{3.13}$$

At distance z_{lam}, the plane wave changes to an expanding spherical wave (figure 3.1). In the Fraunhofer zone, the behavior of the axial pressure field can be derived from the equation 3.11 assuming that $z/r >> kr$ as follows

$$p(z) = \frac{\rho_0 c u_0 k r^2}{2z} = p_0 \frac{S}{\lambda z}, \tag{3.14}$$

where S is the area of the ultrasound transducer.

The determination of the off-axis distribution of the ultrasound pressure field is more complicated and currently numerical methods are used for the analysis. The determination of the ultrasound field is based on a use of Huygen's principle. The ultrasound pressure field is considered to be formed as superposition of the point sources placed side by side over the transducer surface [59]. Various solutions have been introduced for the analysis of the ultrasound field of a planar ultrasound transducer [59, 149, 151, 169]. Currently, when analyzing pulsed ultrasound fields in complex geometries, numerical methods are used to characterize the sound fields [73, 169]. The lateral pressure distribution of short high frequency ultrasound pulse generated with a planar circular transducer (*diam.* = 0.5 mm) is presented in the figure 3.2.

For the pulsed and broadband ultrasound fields used in medical ultrasound applications, the shape of the Fresnel zone differs significantly from that of a continuous single frequency ultrasound field [36]. The difference between pulsed and continuous sound fields becomes significant when the length of the pulse is less than six cycles [86]. In a pulsed field, the pressure variation in the Fresnel zone is decreased [36]. As compared to the Fresnel zone, the differences between continuous and pulsed field are smaller in the Fraunhofer zone. One way to describe the pulsed pressure field in the Fresnel zone is to sum the pressure fields of each frequency component of the pulsed ultrasound field [36]. As the pressure field in the Fresnel zone is dependent on the ultrasound frequency, summing the fields of single frequency components diminishes the total variation of the pressure field amplitude [36].

Attenuation is another phenomenon affecting the shape of the pulsed ultrasound field. The ultrasound field is distorted as a broadband ultrasound pulse is passed through the media because of the frequency dependent attenuation . In figure 3.2 the sound field for a short ultrasound pulse (center frequency of 40 MHz) generated with a planar ultrasound transducer (*diam.* = 0.5 mm) is presented for non-attenuating and attenuating media (α = 0.55 dB/(cm MHz)). The attenuation diminishes the pressure amplitude

and changes the shape of the near field pressure distribution.

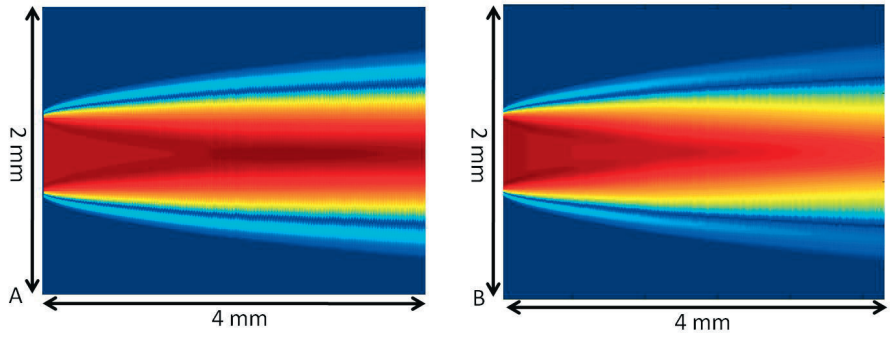

Figure 3.2: Lateral pressure distribution of a high frequency (f = 40 MHz, diam. = 0.5 mm) ultrasound pulse generated by a transducer similar to that applied in the present experimental studies, as it propagates through ***A.*** *a non-attenuating media (ρ = 1000 kg/m^3) and* ***B.*** *an attenuating media (ρ = 1000 kg/m^3, α = 0.55 dB/(cm MHz)).*

3.2.2 Focused transducers

Focused transducers are commonly used to enhance the lateral resolution of ultrasound imaging and to increase the intensity of the ultrasound field. Various methods exist for focusing of ultrasound fields. Electrical focusing is commonly used in medical ultrasound imaging. In electrical focusing, electrical pulses are conducted to a matrix of piezoelectric crystals in a such way that phases the originating ultrasound waves in a desired manner. With this technique, ultrasound field may be focused at various distances from the transducer. If a single crystal is used, the ultrasound field can be focused only by modifying the shape of the ultrasound transducer face or by applying acoustical lenses or mirrors [36]. Similar as in optics, the ultrasound field can be focused using a convex acoustical lens or with a concave acoustical mirror [162]. The downside of the use of lenses and mirrors is that there are always energy losses when ultrasound penetrates through a lens or reflects from a mirror. Furthermore, acoustical mirrors are expensive and, thus, they are only used in difficult geometries when the use of lenses and shaping of

the transducer is not possible [36].

3.3 ULTRASOUND IMAGING

Ultrasound imaging can be conducted in either through-transmission or pulse-echo geometries. In through-transmission geometry, an ultrasound pulse is transmitted with one transducer through an target tissue and the attenuated ultrasound pulse is received by another transducer. With the through-transmission measurements the attenuation and the speed of sound in the tissue can be determined [36]. In the pulse-echo geometry, an ultrasound pulse is transmitted with a transducer and the reflected echo is received with the same or a second transducer [36]. The one dimensional presentation of the reflected ultrasound wave as a function of time is called as A-mode imaging. The time between the transmission and reception of the ultrasound pulse, *i.e.*, time of flight (TOF), can be measured from the A-mode image and if the speed of sound in the tissue is known, the distances between the transducer and the reflector can be determined. A two or three dimensional ultrasound image can be created when the ultrasound transducer is scanned over the region of interest and the location of the reflection is plotted in the x-y coordinates [36]. The amplitude of the ultrasound reflection may be presented as brightness of the spot representing the location of the reflection (B-mode image) [36]. In medical applications ultrasound images are usually generated with phased array transducers where numerous miniaturized ultrasound crystals are located side by side, creating a matrix [36].

The resolution of the ultrasound image is dependent on the dimensions of ultrasound field (*e.g.* focus width and length) and the frequency content and duration of the ultrasound pulse [162]. The dimensions of the ultrasound field and lateral sampling frequency affect the lateral resolution of the ultrasound system, *i.e.*, the smallest distance between two separate targets that can be differentiated in the lateral dimensions of the ultrasound image [162]. The length and frequency content of the ultrasound pulse affect the axial reso-

lution. Axial resolution is defined as the shortest distance between two separate targets on top of each other that can be separated. In theory, the axial resolution of the ultrasound system is a half of the length of the ultrasound pulse. Since the ultrasound attenuation is dependent on the frequency, only the superficial layer of the tissues can be imaged with high frequency ultrasound transducers and, thus, the selection of the ultrasound frequency is always a compromise between the axial resolution and the maximum imaged depth [162].

3.4 INTRAVASCULAR ULTRASOUND TECHNIQUE

The intravascular ultrasound technique is a high resolution clinical imaging technique used for imaging of vascular walls, typically in coronary arteries [120]. The technique is used to detect and evaluate the severity and type of changes related to coronary artery disease. With the IVUS technique, the changes in the structure of artery wall can be detected and the amount and composition of the plaque which has accumulated on the artery walls can be approximated [47, 56, 119, 131]. Furthermore, the areas of the artery and lumen of the artery can be quantitatively measured [120].

An IVUS instrumentation consists of a thin (*diam.* = 1-3 mm) ultrasound catheter incorporating a miniaturized ultrasound transducer and a main unit equipped with a pulser, a receiver and data and image processing hardware. There are two designs for IVUS transducers though the most common design is the mechanically rotating single ultrasound transducer which transmits and receives the ultrasound pulse in specific angles creating cross sectional images of the object. The second design consists of a ring-like phased array of ultrasound crystals which transmit and receive ultrasound pulses individually. The ultrasound frequency applied in the IVUS transducers is typically between 9-40 MHz.

This thesis utilized a non-focused 40 MHz ultrasound catheter incorporating a rotating ultrasound transducer. The ultrasound transducer was rotating at 30 r/s and transmitting and receiving

ultrasound pulse in intervals of 1.4°. The theoretical lateral resolution of this ultrasound instrumentation depends on the distance between the ultrasound catheter and the target surface as well as on the angle between the ultrasound transducer and the target. If one assumes that the scanned surface is flat, then the distance between two scan lines can be calculated as follows

$$d = z \tan \phi, \tag{3.15}$$

where z is the distance between the ultrasound catheter and the imaged surface and θ is the angle between the ultrasound transducer and the imaged surface.

3.5 ULTRASONIC EVALUATION OF ARTICULAR CARTILAGE

Changes in the composition and structure of the articular cartilage related to the cartilage degradation or injuries have a significant effect on the acoustical properties of the tissue [3, 29, 74, 114, 138, 142, 153] and, thus, the integrity of the articular cartilage can be evaluated with quantitative ultrasound measurements. The literature describes various ultrasound methods for estimating the integrity of the articular cartilage. These techniques are based on measurements of the changes in the ultrasound speed, attenuation and backscattering within the cartilage and reflection coefficient and roughness of the articular surface.

The speed of ultrasound in articular cartilage has been shown to depend on both the composition (proteoglycan, collagen and water contents) and the structure of the tissue [3, 116, 152, 153]. In healthy cartilage, the speed of sound varies between 1579-1934 m/s depending on the location [74, 97, 115, 165]. Degeneration of the articular cartilage evokes a decrease in the ultrasound speed of cartilage [74, 116, 127, 153]. The speed of ultrasound in spontaneously degraded human cartilage is about 1560-1600 m/s [110, 152]. It has been proposed that the decrease in the speed of sound is related to the increase of the cartilage water content and the changes in

the orientation of the collagen fiber network [117]. Thus, accurate measurement of the ultrasound speed in cartilage could provide an indirect information of the integrity of the articular cartilage.

The attenuation of ultrasound in the articular cartilage is dependent on the composition and structure of the tissue [117]. It has been reported that the ultrasound attenuation is significantly related to the integrity of the collagen cross links [3] and the collagen and proteoglycan contents of the articular cartilage [114]. Ultrasound attenuation has been reported to vary between species and anatomical locations and also as a function of tissue depth [3, 116, 127]. Furthermore, the spontaneous degeneration of the articular cartilage has been shown to be linked with reduced ultrasound attenuation [114].

Swelling is one of the earliest OA related changes occuring in the cartilage [20]. On the other hand, as the disease progresses, cartilage is gradually worn out and in the final stage the subchondral bone will be exposed. Ultrasound can quantitatively evaluate the changes in the cartilage thickness [29, 142]. However, in the determination of the cartilage thickness, the speed of sound is usually assumed to be constant in cartilage and this can affect the reliability of the measurements.

Ultrasound reflection and backscattering are sensitive indicators of the integrity of cartilage surface [29, 77, 116, 138, 142, 153]. The ultrasound reflection at the articular surface depends on the integrity of collagen network and the roughness of the surface [116, 138]. The degenerative changes in the articular cartilage (*i.e.* disruption of the cartilage surface collagen network and the fibrillation of cartilage surface) decrease significantly (up to 90 % [138]) ultrasound reflection amplitude at the cartilage surface [29, 116, 138, 153]. Furthermore, the amount of ultrasound scattering from the subsurface structures of cartilage tissue has been shown to be related to the integrity of the collagen fiber network within the cartilage [29, 49].

Sclerosis and abnormal remodeling of the subchondral bone can occur already at the early stages of OA [20]. Thus, in the early diagnostics of OA, it is also essential that one could make a quantitative

evaluation of the integrity of the subchondral bone. The sclerosis of subchondral bone can be detected from qualitative ultrasound images [35, 142]. Furthermore, the sclerosis of the subchondral bone can be quantitatively evaluated via the increase in the ultrasound reflection from the cartilage bone interface [139]. However, for reliable measurement of the ultrasound reflection from the subchondral bone, the effect of overlying cartilage layer has to be taken into account.

The fibrillation of the cartilage surface caused by the disruption of the superficial collagen network is one of the earliest signs of OA [20]. The roughness of the cartilage surface can be measured directly or indirectly with ultrasound. Adler *et al*. proposed quantification of cartilage surface roughness based on the measurement of scattering of ultrasound at various angles between the ultrasound transducer and cartilage surface [2]. However, this technique only indirectly measures the surface roughness. In an attempt to achieve a direct measurement of the cartilage surface microroughness the ultrasound roughness index (*URI*) has been introduced [138]. This technique is based on the quantification of the variation of the distance between the cartilage surface and the ultrasound transducer.

In this thesis, ultrasound reflection and backscattering measurements of articular cartilage were conducted. In the following chapter, the most important parameters for the quantification of the reflected and scattered ultrasound will be introduced.

3.5.1 Reflection

Chérin *et al*. introduced a quantitative method for the evaluation of the articular cartilage reflection coefficient in the frequency domain [29]. In order to determine the reflection coefficient, one measures the reflection from the cartilage surface and a perfect reflector with the same acquisition system and at the same distance z from the imaged surface. Their solution includes the following assumptions: 1) The reflection coefficient is frequency independent at the imaged surface, 2) The imaged surface is flat and perpendicular

Table 3.2: Values of reflection coefficient R, integrated reflection coefficient IRC, apparent integrated backscattering AIB and ultrasound roughness index URI of articular cartilage determined with ultrasound. Parameter values without standard deviations are approximated from figures.

Species	**Site**	**Treatment**		*R* **(%)**	*IRC* **(dB)**	*AIB* **(dB)**	*URI* **(μm)**	**f (MHz)**	*n*	**Study**
Bovine										
	PAT	Intact		3.1 ±1.0	-34.2±4.1	-	5.3±2.1	50	8	[77]
				17.7±2.7	-53.1±2.7	-	6.0±1.4	40	20	[159]
				4.4±1.5	-28.0±3.4	-	7.7±1.6	20	8	[138]
				1.7±0.9	-36.4±6.2	-	1.1±0.3	10	8	
				2.4±0.6	-32.5±2.5	-	1.1±0.3	5	8	
		Mechanical	emery paper P60	2.2±0.6	-32.6±2.0	-	28.8±15.1	20	8	[138]
		degradation	emery paper P240	2.5±0.6	-31.0±1.5	-	12.4±2.8		6	
			emery paper P360	2.4±0.7	-31.3±3.0	-	13.3±3.9		6	
		Enzymatic	Collagenase	0.4±0.8	-46.9±2.5	-	34.8±11.8	20	6	[138]
		degradation	Trypsine	3.7±0.6	-28.3±1.2	-	9.0±2.4		6	
			Chondrotinase ABC	4.2±2.7	-29.6±5.1	-	12.4±4.5		6	
	FMC	Intact		2.6	-30.1	-	12.0	20	6	[88]
	LPG			2.5	-31.0	-	14.4		6	
	MTP			1.6	-33.7	-	16.2		6	
Rat										
	PAT	Enzymatic	control	-	-20.9	40.3	-	55	9	[128]
		degradation	Sodium acetate	-	-20.6	40.1	-		9	
		Maturation	5 weeks	-	-21.2	40.9	-	53	8	[30]
			6 weeks	-	-23.2	43.1	-		8	
			8 weeks	-	-21.4	47.9	-		8	
			11 weeks	-	-24.0	50.0	-		8	
	FH	Intact		-	-28.7±2.6	-23.1±1.4	3.5±0.9	40	12	[157]
	MFC			-	-28.8±1.4	24.7±2.4	2.8±0.3		12	
	LFC			-	-29.7±2.6	24.8±3.9	3.5±0.9		12	
	PFG			-	-28.5±3.3	24.2±2.8	3.2±0.6		12	
	PAT			-	-33.7±3.5	26.9±2.9	4.0±1.8		12	
Porcine	FT	Repair	Control	6.2	-	-	7.5	20	5	[90]
			Lesion	1.6	-	-	44.0		8	
			Adjacent to lesion	4.4	-	-	10.0		8	
Miniature pig	FT	Repair	Control	-	-18.0	-	-	50		[49]
			Lesion	-	-15.8	-	-			

PAT = patella FMC = femoral medial condyle LPG = lateral patello-femoral groove
MTP = medial tibial plateau FH = femoral head MFC = medial femoral condyle
LFC = lateral femoral condyle PFG = patello-femoral groove

to the ultrasound transducer, 3) The distance z between the ultrasound transducer and the imaged surface is large enough ($z >> a$) as compared with the dimensions of the ultrasound transducer, 4) The dimensions of the imaged surface are small as compared with the distance between the imaged surface and the ultrasound transducer. If these assumptions are valid then the ultrasound signals reflected from saline cartilage ($S_C(z,f)$) and saline perfect reflector ($S_c(z,f)$) interfaces can be presented in the frequency domain as follows:

$$S_c(z,f) = E(f) \times G(f) \times A_0(z,f) \times H^2(z,f) \times R_c(f) \quad (3.16)$$

$$S_r(z,f) = E(f) \times G(f) \times A_0(z,f) \times H^2(z,f) \times R_r(f), \quad (3.17)$$

where $E(f)$ is the acoustoelectric transfer function, $G(f)$ is the acquisition system transfer function, $A_0(z,f)$ is the frequency and depth dependent attenuation function in physiological saline, $H^2(z,f)$ is the diffraction function, $R_c(f)$ is the frequency dependent cartilage reflection coefficient and $R_r(f)$ is the frequency dependent reflection coefficient of the perfect reflector. Assuming that $R_r(f)$ is independent of frequency and equal to 1, the frequency reflection coefficient of the cartilage can be written as follows:

$$R_c = \frac{S_c(z,f)}{S_r(z,f)}, \quad (3.18)$$

where $S_c(z,f)$ and $S_r(z,f)$ are determined by means of the Fourier transform. In order to enhance the proportion of the specular reflection the signal is Hamming windowed before the Fourier transformation. The energy reflection coefficient is defined in the dB scale as follows:

$$R_c^{dB}(f) = 10 \times \log_{10} \left\langle |R_c(f)|^2 \right\rangle, \quad (3.19)$$

where $\langle \dots \rangle$ indicates the spatial mean of all scan lines in the ultrasound image. Finally, the integrated reflection coefficient (IRC) may be determined as follows

$$IRC = \frac{1}{\Delta f} \int_{\Delta f} R_c^{dB}(f) df, \quad (3.20)$$

where Δf indicates the -6 dB frequency bandwidth of the ultrasound transducer.

The ultrasound reflection can be determined also in the time domain. With the same assumptions, the ultrasound reflection coefficient may be determined as a ratio of the peak-to-peak amplitude of a pulse reflected from the saline-cartilage interface (A_c) and the peak-to-peak amplitude reflected from the saline-perfect reflector interface (A_r)

$$R_c = \frac{A_c}{A_r} \cdot 100\%. \tag{3.21}$$

3.5.2 Backscattering

Chérin et al. introduced a method for the quantification of the echogenecity of cartilage inner structures [29]. Similarly to the previous chapter, the effect of the acquisition system, and diffraction and attenuation on the measured ultrasound signal must be eliminated by normalization of the frequency domain signal $S_B(z,f)$ being measured from the cartilage inner structures with the frequency domain signal measured from the perfect reflector at the corresponding distance. The frequency dependence of the apparent backscattered energy is defined as

$$\mu_c = \frac{S_B(z,f)}{S_r(z,f)}, \tag{3.22}$$

where $S_B(z,f)$ and $S_r(z,f)$ are determined by means of the Fourier transformation. Frequency domain apparent backscattered energy μ_c^{dB} is determined in the decibel scale as follows

$$\mu_c^{dB}(f) = 10 \times \log_{10} \left\langle |\mu_c(f)|^2 \right\rangle, \tag{3.23}$$

where $\langle \dots \rangle$ indicates the spatial mean of all scan lines in the ultrasound image. Finally, the apparent integrated reflection coefficient (AIB) is determined as follows

$$AIB = \frac{1}{\Delta f} \int_{\Delta f} \mu_c^{dB}(f) df, \tag{3.24}$$

where Δf refers to the - 6 dB frequency bandwidth.

3.5.3 Ultrasound roughness index

In attempts to detect the fibrillation of the cartilage surface, quantitative methods have been developed for the measurement the cartilage surface roughness. Saarakkala *et al*. introduced the ultrasound roughness index (URI) for direct quantification of the cartilage surface roughness [138]. URI is determined by calculating the root mean square value of the difference in distance between the cartilage surface and the ultrasound transducer at a single measurement point and average distance between the ultrasound transducer and the cartilage surface

$$URI = \sqrt{\frac{1}{m}\sum_{i=1}^{m}(d_i - \langle d \rangle)^2}, \tag{3.25}$$

where m is the number of measurement points, d_i is the distance between the cartilage surface and the ultrasound transducer in i:th measurement point and $\langle d \rangle$ is the average distance between the cartilage surface and the ultrasound transducer [138].

In the determination of URI, the cartilage surface is assumed to be flat and perpendicular to the incident ultrasound pulse [138]. Since the cartilage surface is always slightly curved, its effect on the values of URI must be eliminated by using trend removal algorithms [138]. In the calculation of URI, the most common trend removal techniques are polynomial fitting, high pass filtering and fitting of smoothing spline functions.

4 Optical coherence tomography

Optical coherence tomography (OCT) is a relatively new high resolution, non-invasive three dimensional imaging technique used in various medical imaging applications, *e.g.* in ophthalmology and cardiology. The advantages of OCT as compared with clinical ultrasound or MRI techniques are its superior resolution and low cost. In this chapter, the basics of light and matter interactions, optical coherence tomography and optical evaluation of articular cartilage will be introduced.

4.1 LIGHT AND MATTER INTERACTIONS

The speed of light in a vacuum is a physical constant but in a medium it will vary according to its material properties. The ratio of speed of light in the vacuum and in the media is indicated by the refractive index. Similar to acoustics, the refractive index defines the proportion of light reflection at the interface of two optically different materials.

As light propagates in a tissue the intensity of the light is decreased by absorption and scattering processes [27]. The shape of scattering pattern is described with a parameter called the anisotropy coefficient g. The values of g vary between -1 and 1, where values -1, 0 and 1 of g represent extremely forward, isotropic and highly backward scattering, respectively [27].

In some tissues, the polarization state of light changes as it propagates through material. This effect is called birefringence. Birefringence in tissues can be traced to the anisotropic properties of tissue molecules such as hydroxyapatite crystals in dental enamel or to structural anisotropy such as in the case of the collagen fibers in

articular cartilage [46].

4.2 BASICS OF OPTICAL COHERENCE TOMOGRAPHY

The basic principle of OCT is analogous to ultrasound imaging with the exception that near infrared light is used instead of sound waves. Thus, OCT imaging is based on the measurement of light reflection and scattering from the imaged tissue. OCT measurements and image reconstruction can be implemented by using various techniques. Here, time domain, frequency domain and polarization sensitive OCT techniques will be briefly introduced. The time domain OCT (TD-OCT) is the most widely applied OCT technique. TD-OCT is based on the measurement of light interference in various light path lengths enabling depthwise scans of the imaged tissue. The basic design of the TD-OCT technique is illustrated in Figure 4.1.

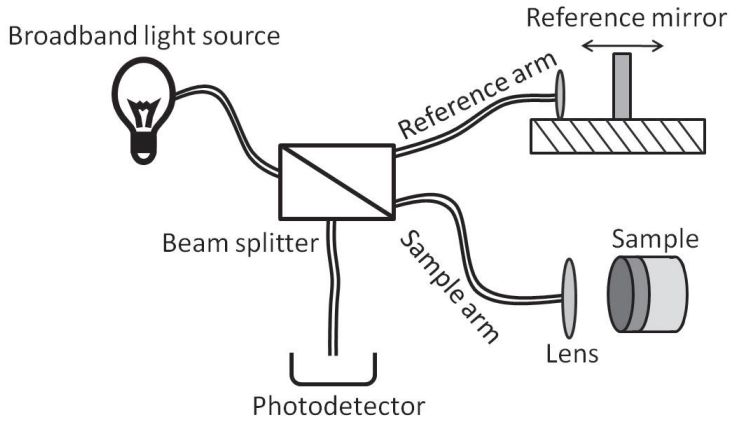

Figure 4.1: Basic design of the measurement set-up applied in the TD-OCT technique

In the TD-OCT, technique the light from a broadband light source is split into two beams in the beam splitter. One beam travels to the reference arm where it is reflected from a reference mirror. The second beam passes to the sample arm where it is reflected and scattered from the tissue. Interference is detected as the light path

lengths of the reference and sample arms are matched within half of the coherence length of the light source. By gradually moving the reference mirror, a depth-wise scan of the reflection inside the tissue is obtained [150]. Since the axial resolution of the OCT device is related to the coherence length of the light in use, broadband light sources with a short coherence length are used [130].

Frequency or Fourier domain OCT (FD-OCT) eliminates the need for depth scanning. In FD-OCT, the reference path length is fixed and the photodetector has been replaced with a spectrometer [150]. The modulation of the intensity spectrum detected with a spectrometer is proportional to the optical path difference between the arms. The detected intensity spectrum is inversely Fourier transformed into the time domain in order to reconstruct the depth-resolved optical structures of the sample. The advantage of FD-OCT is that the depth-wise scans can be reconstructed from a single exposure, which enables the use of high frame rates. Furthermore, with FD-OCT one can achieve significantly higher (+20 dB) signal-to-noise ratio as compared to that obtained with TD-OCT [150].

Polarization sensitive OCT (PS-OCT) devices have been developed for the evaluation of changes in the polarization state of light after propagating through soft tissue. The change in the polarization state can occur due to birefringence or scattering within the tissue [150]. The design of the PS-OCT devices is similar to that of the TD-OCT and FD-OCT devices, with an additional linear polarizer after the light source, a polarizing beam splitter, and an extra photodetector in the output arm [150]. PS-OCT is attractive for medical imaging because it provides an extra contrast mechanism that could aid in the diagnosis of certain pathologies [150].

4.3 OPTICAL EVALUATION OF ARTICULAR CARTILAGE

OCT is a potentially useful technique for the clinical evaluation of the integrity of articular cartilage. The main advantage of OCT compared to the other clinically applicable imaging methods is its high resolution being typically 10-15 μm [48]. OCT imaging has

been used for the evaluation of cartilage thickness, surface reflection and roughness [57]. Furthermore, with the PS-OCT technique, the disorganization of the collagen network can be qualitatively evaluated [164]. Currently, there is an interest for the development of quantitative optical parameters for evaluation of the OA-related changes in articular cartilage.

The thickness of the articular cartilage can be quantitatively evaluated from an OCT image [57, 66]. However, because of extensive scattering, the light penetrates only 2-3 mm into the soft tissues which limits the usefullness of OCT for the determination of human cartilage thickness [48]. The organization of the collagen network within the cartilage has also been quantitatively evaluated with PS-OCT [32, 164]. Furthermore, the reflection coefficient and microroughness of the cartilage surface can be quantitatively evaluated [57, 141, 158].

The essential optical parameters related to OCT will now be briefly reviewed. Saarakkala *et al*. introduced an optical reflection coefficient (*ORC*) for the quantification of the optical reflection at the cartilage surface (Equation (4.1)) [141]. In the determination of *ORC*, the effect of the acquisition system on the determined reflection coefficient is eliminated by the normalization of the cartilage reflection with the reflection from a reference reflector with a known optical refractive index [67, 141].

$$ORC = \frac{A_i}{A_{i,c}}. \tag{4.1}$$

Huang *et al*. introduced an optical backscattering (*OBS*) parameter (Equation (4.2)) for the quantification of the amount of light scattered within cartilage tissue [67]. *OBS* is defined as the mean optical signal value measured for the cartilage inner structures corrected with the optical reflection at the cartilage surface [67].

$$OBS = \frac{1}{\left(1 - ORC_i^2\right)^2} \bar{b_i^2}, \tag{4.2}$$

where, $\bar{b_i}$ is the mean value of the optical signal recorded from the

cartilage inner structures and ORC_i is the optical reflection coefficient at the cartilage surface.

Saarakkala *et al*. devised an optical roughness index (Equation (4.3)) for the determination of the microroughness of the cartilage surface. The parameter is analogous to the ultrasound roughness index developed for the determination of microroughness from 2D ultrasound images [138]. ORI is defined as follows:

$$ORI = \sqrt{\frac{1}{m}\sum_{i=2}^{m}\left(d_i - \bar{d}\right)^2}, \tag{4.3}$$

where m is the number of scan lines in a 2D OCT image, d_i is the distance between the OCT probe and the cartilage surface at the i^{th} scan point and $\bar{d}$ is the average distance between the OCT probe and the cartilage surface.

To quantify microroughness, the trend arising from the natural curvature of the cartilage surface is removed from the measured profiles before determination of the values of ORI [141]. For example the trend can be removed by lowpass filtering or by reducing a polynomial or smothing spline function fitted to the recorded surface profile.

5 Aims

This thesis work introduces a novel arthroscopic ultrasound technique for diagnostics of cartilage injuries and degeneration. The technique was initially evaluated *in vitro* with artificially degraded cartilage, further tested with spontaneously and surgically repaired animal cartilage *in vitro* and *ex vivo* and finally applied clinically *in vivo*.

The specific aims of this thesis were:

1. To develop a novel arthroscopic ultrasound imaging technique and to evaluate its potential in detecting artificial degradation of articular cartilage *in vitro*
2. To investigate the potential of the arthroscopic ultrasound technique for evaluation of the integrity of surgical repair of cartilage *in vitro*
3. To compare the potential of ultrasound and OCT techniques in the evaluation of the integrity of spontaneously healed articular cartilage *in vitro*
4. To evaluate the potential of the novel ultrasound technique to distinguish between a mechanical cartilage lesion and intact tissue in arthroscopic conditions *ex vivo*
5. To investigate the potential of the arthroscopic ultrasound technique to evaluate the integrity of human articular cartilage *in vivo*

6 Materials and Methods

This thesis consists of five independent studies (I-V). Summary of the materials and methods is presented in the Table 6.1

Table 6.1: Summary of the materials and methods used in the thesis

Study	Samples	*n*	Methods	Parameters
I	Bovine patella	13	Ultrasound imaging	*R*, *IRC*, *URI*
	Intact	13	Light microscopy	Qualitative
	Mechanically degraded	7	SEM	Qualitative
	Enzymatically degraded	6	Histology	Mankin scoring
II	Rabbit femoral sulcus	13	Ultrasound imaging	*R*, *IRC*, *AIB*, *URI*
	Intact	13	Light microscopy	Qualitative
	Surgical repair	8	PLM	Qualitative
	Spontaneously healed	5	Histology	O'Driscoll scoring
III	Horse os carpale III and IV	7	Ultrasound imaging	*IRC*, *AIB*, *URI*
	Intact	14	OCT	*ORC*, *OBS*, *ORI*
	Adjacent	56	Biomechanics	E_{eq}, E_{dyn}
	Injured	56	PLM	Qualitative
			DD	Optical density
IV	Bovine patella	7	Ultrasound imaging	*R*, *IRC*, *AIB URI*
	Femoral sulcus	7	Biomechanics	Stiffness
	Intact	7	Light microscopy	RMS roughness
	Mechanically degraded	7	Histology	Mankin scoring
V	Human knee	7	Ultrasound	*R*, *IRC*, *AIB URI*
			Arthroscopy	ICRS scoring, Ultrasound scoring

RMS = Root mean square
SEM = Scanning electron microscopy
DD = Digital densitometry
R = Time domain reflection coefficient
ORI = Optical roughness index
E_{eq} = Equilibrium modulus
URI = Ultrasound roughness index
PLM = Polarized light microscopy
AIB = Apparent integrated backscattering
OCT = Optical coherence tomography
ORC = Optical reflection coefficient
OBS = Optical backscattering
IRC = Frequency domain reflection coefficient
E_{dyn} = Dynamic modulus
ICRS = International cartilage repair society

6.1 ARTICULAR CARTILAGE SAMPLES AND PHANTOMS

In studies I and IV, bovine knee articular cartilage obtained from a local slaughterhouse (Atria Oyj, Kuopio, Finland) was used. In study I, the knee joints were opened within a few hours *post mortem* and cylindrical osteochondral plugs (*diam.* = 25.4 mm) were prepared from visually intact lateral upper quadrants of bovine patellae. After ultrasound imaging, the osteochondral samples were subjected to either mechanical degradation with emery paper (grit number 60, FEPA standard average particle *diam.* = 269 μm) or to specific enzymatic degradation of collagen (Collagenase Type 1a, C9891, Sigma Aldrich, 110 U/ml for 18 h). Subsequently, samples were imaged again with ultrasound and prepared for histological analyses. In addition, in study I, emery papers (n = 8) of variable roughness (FEPA standard, average particle sizes 269 μm, 125 μm, 58.5 μm, 46.2 μm, 40.5 μm, 21.8 μm, 8 μm and 5 μm) were used as phantoms. For this purpose, the emery papers were glued onto plastic blocks prior to ultrasonic scanning. In study IV, visually intact bovine knee joints were investigated under arthroscopic conditions *ex vivo*. Under arthroscopy (lens inclination 0°, diameter of arthroscope = 4 mm, 20207 A, Karl Storz GmbH & Co, Tunningen, Germany), a mark of approximately 10-20 mm in length and 0.5-1.0 mm in depth was created with a curet to the distal central patella and distal femoral sulcus. Subsequently, the cartilage surface adjacent to the mark was mechanically degraded by inserting a custom-made steel brush into the joint and rubbing the cartilage surface in order to create a low grade cartilage injury. After the measurements, cylindrical osteochondral plugs (*diam.* = 25.4 mm), including the damaged and intact tissue, were extracted from the measurement sites and prepared for histological analyses.

In study II, healing of the surgically injured rabbit knee cartilage was investigated in two different groups: 1) surgically repaired and 2) spontaneously healed articular cartilage. The intact adjacent cartilage near the lesion sites was used as a reference tissue. In attempt to simulate an injury, an osteochondral lesion of 4 mm in diameter

and 3 mm in depth was drilled into the patellar groove of a New Zealand rabbits (n = 13). Subsequently, the lesions were either allowed to heal spontaneously, or were repaired using gel containing recombinant human type II collagen (3.7 mg/ml) and chondrocytes (10×10^6/ml), extracted from the same animal. The animals were sacrificed after 6 months of healing and osteochondral specimens were collected from the repair sites. Subsequently, the samples were stored in a freezer (-20°C) until the experiment. The Institutional animal care and use committee of the University of Kuopio and the provincial government approved these animal experiments (license number 04-82).

In study III, osteochondral lesions of 8 mm, 6 mm, 4 mm and 2 mm in diameter were surgically created in one of the intercarpal joints (os carpale III and IV) of a 24 month old horse. Chondral lesions were created in similar manner on the contralateral joint. The lesions were allowed to heal spontaneously for 12 months. After sacrificing the horse, ostechondral plugs (*diam*. = 14 mm) that included the lesion and intact adjacent tissue were harvested and stored at -20° until further processing. The intact adjacent cartilage tissue near to the lesion sites was used as a control. The procedures were approved by the Utrecht University Animal Experiments Committee as required under Dutch legislation.

Study V consisted of seven patients undergoing arthroscopic surgery of the knee as treatment or examination of their joint disease or condition. The indication for conducting an arthroscopy was a suspicion of articular or meniscal lesion, such as meniscal tear, chondral lesion, osteoarthritis or loose body. The measurement sites were patella, femoral sulcus, medial and lateral condyle of femur and medial and lateral facets of proximal tibia. The study was in compliance with the ethical guidelines of the appropriate institutions.

6.2 ULTRASOUND IMAGING

6.2.1 *In vitro* experiments

A clinical high resolution intravascular ultrasound (IVUS) system (Clear View Ultra, Boston Scientific Corporation, San Jose, CA, USA) and high frequency ultrasound catheter (center frequency = 40 MHz, -6 dB bandwidth = 30.1 to 45.3 MHz; pulse length = 0.124 μs; beam dimensions (-6 dB) = 0.417 mm and 0.523 mm in x and y direction, respectively) (Atlantis^{TM} SR Pro, Boston Scientific Corporation, San Jose, CA, USA) were used in all studies (Figure 6.1). The IVUS catheter (*diam.* = 1 mm) incorporated a miniature, (*diam.* = 0.5 mm) unfocused, rotating (30 rps, each revolution consisting of 255 scan lines) transducer. In Studies I-III, the ultrasound catheter was fixed to the motorized high resolution drives which permitted precise control of the positioning of the ultrasound transducer (Figure 6.1).

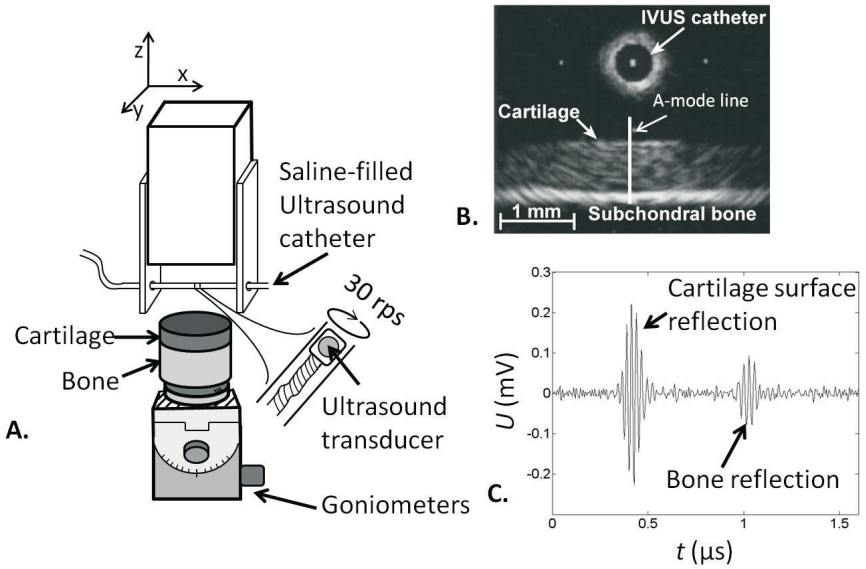

Figure 6.1: ***A****. The in vitro measurement geometry used in studies I-III.* ***B****. A representative 2D ultrasound image of bovine patellar articular cartilage and subchondral bone.* ***C****. A typical A-mode ultrasound acquisition.*

6.2.2 *Ex vivo* and *in vivo* experiments

In studies IV and V, the ultrasound measurements were conducted under arthroscopic control (Figure 6.2). The ultrasound catheter was inserted into the knee joint using the anteromedial and anterolateral portals. In order to protect the ultrasound catheter from damage, it was inserted into the joint through a metallic tube (*diam.* = 5 mm). The position of the ultrasound probe was monitored through an arthroscope. The angle between the rotation plane of the ultrasound probe and cartilage surface was manually adjusted to be perpendicular in order to record the maximum ultrasound reflection. This was achieved by visually monitoring the magnitude of the cartilage surface reflection from the display of the IVUS device. The distance between the transducer and cartilage surface was monitored by the aid of the display of the IVUS device and adjusted to be approximately 2 mm. When the position of the ultrasound catheter was optimal (*i.e.*, the maximum reflection was detected) ten full revolutions of the ultrasound probe were recorded and the revolution with the highest reflection was stored for later analysis. In study IV, all the measurements were repeated six times and the three measurements with the highest reflection values were selected for the analysis. In study V, the measurements were repeated three times and the best measurement was selected for subsequent analysis.

In all studies, the radiofrequency (RF) ultrasound signals were acquired with a 250 MHz sampling frequency from the RF output of the IVUS main unit using a digital oscilloscope (Wave Runner 6051A, LeCroy Corporation, Chestnut Ridge, NY, USA). The acquired signal was stored for off-line analysis using a custom-made LabView-software (version 8.2, National Instruments Corporation, Austin, TX, USA).

In study V, the ultrasound score was determined for each measurement site from ultrasound images by one of the operating surgeons. The ultrasound score is similar to the ICRS scoring system [18] excluding the scoring of the cartilage stiffness.

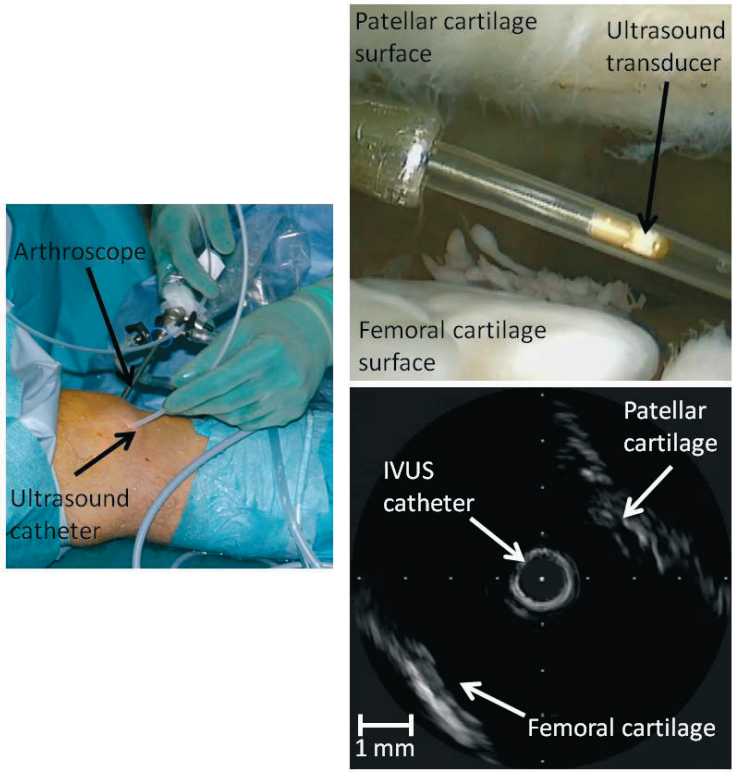

Figure 6.2: The in vivo measurement geometry. Ultrasound examination was carried out using the same anteromedial and anterolateral portals that were used in routine arthroscopy. The ultrasound transducer was guided to the measurement site with the help of the arthroscope. When the position of the ultrasound catheter was optimal (i.e., the maximum reflection was detected) ten full revolutions of the ultrasound probe were recorded and the revolution with the highest reflection was stored for later analysis. In addition to the ultrasonic data, a digital video from the arthroscopy was recorded through the arthroscope.

6.3 OCT MEASUREMENTS

The OCT measurements (study III) were conducted with a custom-made single-channel time-domain OCT system equipped with a 1310 nm super luminescent diode (bandwidth 50 nm, corresponding to an axial resolution of approximately 15 μm) and a vertically adjustable scanning probe incorporating an optical fiber, a compound lens and a scanning mirror. The OCT signal was collected from the device with custom-made LabView (version 8.2 National Instruments Corporation) software and digitized (sampling frequency = 500 kHz) with a data acquisition card (PCMCIA 6062E, National Instruments corporation). Data was stored for the off-line analysis to be conducted with a custommade Matlab (Matlab 7.0.4, Mathworks Inc., Natick, MA, USA) program.

6.4 QUANTITATIVE ULTRASOUND AND OPTICAL PARAMETERS

6.4.1 Reflection and backscattering parameters

Ultrasound reflection from the cartilage surface was quantified in studies I, II, IV and V by the integrated reflection coefficient (IRC) and the reflection coefficient (R) (Equations 3.20 and 3.21, respectively). In study III, the ultrasound reflection from the cartilage surface was quantified by determining only IRC. In this analysis, ten 360 degree sweeps (ten full rotations of the IVUS probe) were recorded. Acquisitions with the angle of incidence of 89.3 - 90.7 degrees were accepted for analysis. This was achieved by selecting the ultrasound signal with the smallest TOF-value. In the axis parallel to the long axis of the catheter, the perpendicularity was ensured by searching for the maximal reflection amplitude using a 3D angular adjustment system (Figure 6.1). Before the calculations the RF-ultrasound signal was bandpass filtered (a 50^{th} order digital FIR filter, pass band 15 - 80 MHz) and before calculation of IRC, the signal was Hamming windowed (0.4 μs window) [29].

In studies II-V, ultrasound backscattering was quantified by de-

termining AIB (Equation (3.24)), assessed at the same scan line as the R and IRC. In the determination of AIB, a rectangular window (length = 0.48 s) was selected under the cartilage surface.

A reference signal was recorded at the saline steel interface to calculate the absolute values of ultrasound reflection and backscattering parameters (R = 93.7 %). In studies I-III, the reference reflection was recorded at the same distance as the cartilage surface reflection. In studies IV and V, the reference reflection was recorded at various distances (1-4 mm, 30 measurement distances) between the surface of the steel plate and the ultrasound catheter. For each arthroscopic measurement, the reference reflection from the saline-steel interface at the nearest distance to that of the saline-cartilage reflection was selected for the normalization of the reflection and backscattering parameters.

In study III, the optical reflection coefficient (ORC) of cartilage surface was quantified using Equation (4.1). The ORC value was determined as a spatial average of 100 recordings at the cartilage surface (spatial resolution 0.01 mm, length of the scan line 1 mm). The optical backscattering (OBS) was determined as the average signal scattered within an approximately 500-point (about 0.5 mm) region under the surface of the cartilage (Equation (4.2)).

In the calculation of the absolute values of optical reflection and backscattering parameters, a reference signal was recorded from an air-glass interface and the reference signal values were corrected to correspond to those of a perfect reflector by using the theoretical refractive index of glass. The reference signal was used for normalization of cartilage reflection according to Equation (4.1).

6.4.2 Surface roughness parameters

In order to determine the ultrasound roughness index (URI, Equation (3.25)), a cartilage surface profile (length approximately 5 mm) consisting of 11 points (5 points at each side of the point perpendicular to the ultrasound probe) was recorded. In study I, the location of the cartilage surface was determined with the cross-correlation

method [26]. In studies II-V, the location of the cartilage surface was determined as the maximum of the Hilbert envelope of the ultrasound waveform reflected from the cartilage surface. Before the calculation of *URI* the trend arising from the rotation of the ultrasound probe and the natural curvature of the cartilage surface was removed with the smoothing spline fitting technique.

To calculate *ORI*, the cartilage surface location was determined at each measurement point. This was achieved by calculating the absolute values of the Hilbert transformed signal reflected from the cartilage surface and detecting the maximum of the Hilbert envelope at each point. This information was used to create a 100 point long profile of the cartilage surface. Before calculating the *ORI*, the trend arising from the natural curvature of the cartilage surface was removed from the surface profile by high pass filtering of the measured profile (the Butterworth high-pass filter).

6.5 REFERENCE METHODS

6.5.1 Mechanical testing

In study III, the mechanical measurements were conducted with a custom-made high precision material testing device (resolution for deformation and force, 0.1 μm and 5 mN, respectively) [153]. The creep response of the osteochondral samples was determined in indentation geometry (impervious cylindrical indenter, diam. = 0.5 mm). After 0.37 MPa step stress (ramp speed = 15 μ/s), the creep data was recorded until equilibrium (1200 s). A total of three steps was conducted. With dynamic and equilibrium moduli being determined from the creep data, the equilibrium moduli was determined as the slope of the linear fit to the equilibrium points, whereas the dynamic modulus was determined as the stress/strain-ratio from the dynamic phase of the second step. The equilibrium and dynamic modules values were determined by assuming cartilage as being linearly elastic material having dynamic and equilibrium Poisson ratios of 0.5 and 0.1, respectively [65,75].

In study IV, the dynamic stiffness of the cartilage samples was

measured with an arthroscopic indentation instrument (Artscan 200, Artscan Oy, Helsinki, Finland). The indentation instrument consists of a handle and a hollow rod (*diam.* = 5 mm) which has a flat reference plate (*diam.* = 3 mm, *height* = 0.48 mm) and a spherical ended indenter (*diam.* = 0.6 mm, *height* = 0.14 mm) at its distal end. The indenter is pressed against the cartilage surface and the forces on the indenter and the reference plate were measured with strain gauges. When the reference plate force increased above the pre-set value (5 N) the indenter produced a constant deformation of 140 μm on the cartilage surface. Simultaneously, the force by which cartilage resisted the deformation was measured [93]. At each measurement site six indentations were undertaken and the four highest indenter forces were averaged to indicate the cartilage stiffness.

6.5.2 Microscopy

In study I, the surfaces of artificially degraded cartilage samples were imaged with scanning electron microscopy (SEM). Before the SEM, the samples were fixed in 2% glutaraldehyde buffered (pH 7.4) with cacodylate (0.1 mol/l), dehydrated in an ascending series of ethanol solutions, dried using the critical point technique and coated with a sputtered gold layer [76]. The SEM images were used for the qualitative evaluation of the severity of surface degradation.

In studies I-IV, Safranin-O stained sections (thickness = 3 μm) were extracted from the measurement sites and imaged with an optical microscope (Studies I-II: Nikon Microphot FXA, Nikon Corporation, Tokyo, Japan) (Study IV: Stereomicroscope, Carl Zeiss MicroImaging GmbH, Göttingen, Germany). In studies I and IV, the histological sections of the samples were graded using the Mankin scoring method by three of investigators [95]. The final Mankin score of the sample, was obtained by averaging the three scores and rounding up to the nearest integer. In study II, light microscopic images of cartilage sections were graded by using the O'Driscoll grading system [123]. In study IV, the RMS roughness of the cartilage surface was evaluated from the microscopic images. The sur-

face profile was detected from microscopical images and the natural curvature of the cartilage surface was removed from measured profile with a trend removal algorithm. Subsequently, the surface roughness was calculated as the standard deviation of the surface profile.

In studies II and III, the organization of the collagen network was evaluated from non-stained sections by using a polarized light microscope (Leitz Ortholux II POL, Leitz Wetzlar, Wetzlar, Germany). The parallelism index of collagen fibrils was calculated for each pixel in the image [136]. The PLM images were used in the qualitative evaluation of the integrity of the cartilage collagen network.

6.6 STATISTICAL ANALYSES

The statistical analyses in the studies I-V were conducted using the SPSS 14.0 software (SPSS Inc., Chicago, IL, USA).

In the study I, the non-parametric Wilcoxon signed rank test was used to test the statistical significance of difference between the ultrasound parameters determined before and after the mechanical degradation or enzymatic digestion. The limit of statistical significance was set to $p < 0.05$. The correlation between the different ultrasound parameters was evaluated by determining the Spearman's rank correlation coefficient.

In study II, the statistical significance of the difference between the ultrasound parameters determined for the lesion and control sites was tested with the non-parametric Wilcoxon signed rank test. The statistical significance of difference between the histological scores (O'Driscoll) was determined with the Mann-Whitney U-test.

In study III, the statistical significance of difference between the ultrasound and OCT parameters determined for the lesion and control sites was tested with the Wilcoxon signed rank test. The strength of correlation between the different ultrasound and OCT parameters was determined via the Spearman's rank correlation coefficient.

In study IV, the statistical significance of the differences in ultrasound parameters between the degraded and intact sites was tested using the Wilcoxon signed rank test. The measurements conducted from patellar and femoral cartilage were analysed separately. Since the normality of the distribution of the parameters could not be confirmed, the strength of relations between the ultrasound parameters, Mankin score values and mechanical parameters were determined by using Spearman's rank correlation coefficient.

In study V, the correlation between the ultrasound parameters and the ICRS scoring was determined using Spearman's rank correlation coefficient.

In studies I-IV, reproducibilities of the measurements were evaluated by determining the coefficient of variation (CV (%), [54]) and standardized coefficient of variation (sCV (%), [14]). The reproducibilities were determined by repeating all measurements three times at each measurement site. The sCV values were determined by normalizing the CV values with the range of variation of the parameter values in the present sample population. Thus, the sCV values provide a more realistic estimate for the effect of measurement reproducibility on the diagnostic utility of a parameter.

7 Results

The most significant results of studies I-V are summarized in this chapter. The detailed results can be found in studies I-V.

7.1 TESTS WITH PHANTOMS AND CARTILAGE SAMPLES

The IVUS technique was found to be sensitive for assessing artificial degeneration of articular cartilage (Table 7.1). Cartilage surface reflection decreased after mechanical or enzymatical degradation with collagenase ($p < 0.05$). Furthermore, URI increased after mechanical degradation ($p < 0.05$). A significant correlation was found between the ultrasound reflection parameters and URI (r = -0.86, p = 0.018, n = 14). Degeneration of the surface of the cartilage, especially the collagen network, was clearly visible in the SEM and densitometric images (Study I, Figure 2). In addition, after collagenase digestion, significant depletion of cartilage proteoglycans was detected in the densitometric images. In light microscopic images of cartilage surfaces, the mechanical degradation was clearly visible, but no enzymatic digestion could be visualized. The reproducibilities (CV, sCV) of the ultrasound parameters ranged form good to moderate (1.4 - 20.9%).

Ultrasound imaging revealed statistically significant differences among the emery paper phantoms. The dependencies between the nominal particle size and the ultrasound reflection and roughness parameters were linear up to a particle size of 120 μm. In the linear part of the plot, significant linear correlations were detected between the average particle size of emery papers and the ultrasound reflection and roughness parameters (r = -0.86 and r = 0.90, respectively).

With OCT and 40 MHz ultrasound, the surface characteristics of spontaneously degenerated human tibial plateau cartilage could be visualised more accurately than when using an ultrasound fre-

Table 7.1: Ultrasound reflection (R, IRC) and roughness (URI) parameters determined before and after experimental degradation (mechanical or enzymatic with collagenase). All parameters distinguished statistically significantly the degraded samples from the intact tissue.

		Intact	Degraded	Change (%)
Mechanical degradation				
(n = 7)	R (%)	6.8 ± 1.5	2.1 ± 0.5*	-69.1
	IRC (dB)	-23.4 ± 2.0	-34.3 ± 1.7*	-46.6
	URI (μm)	5.9 ± 2.8	20.4 ±5.6*	245.8
Enzymatic digestion				
(n = 6)	R (%)	8.5 ± 1.2	1.2 ± 0.8*	-85.9
	IRC (dB)	-21.6 ± 1.3	-41.5 ± 8.6*	-92.1

*$p < 0.05$, the non-parametric Wilcoxon signed rank test

quency of 9 MHz. However, with 9 MHz ultrasound, the reflection and scattering from the subchondral bone could be visualized (Figure 7.1).

7.2 EVALUATION OF REPAIRED ARTICULAR CARTILAGE WITH ULTRASOUND AND OCT

Surgical or spontaneous cartilage repair could be quantitatively discerned from intact adjacent tissue with the arthroscopic ultrasound technique (Table 7.2 and 7.3). Furthermore, the spontaneously repaired horse cartilage could be distinguished from intact adjacent tissue with OCT (Table 7.3). The ultrasound reflection parameters (R, IRC) displayed lower values in surgically or spontaneously healed tissue than in adjacent intact cartilage. Furthermore, surface roughness (URI) and ultrasound backscattering (AIB) parameters were significantly higher in the surgically or spontaneously healed tissue than in the control tissue. The optical reflection was lower in the spontaneously repaired horse cartilage than in the intact adjacent tissue. The optically determined surface roughness (ORI) was higher in spontaneously repaired tissue than in intact adjacent tissue. Furthermore, the optical backscattering was also higher

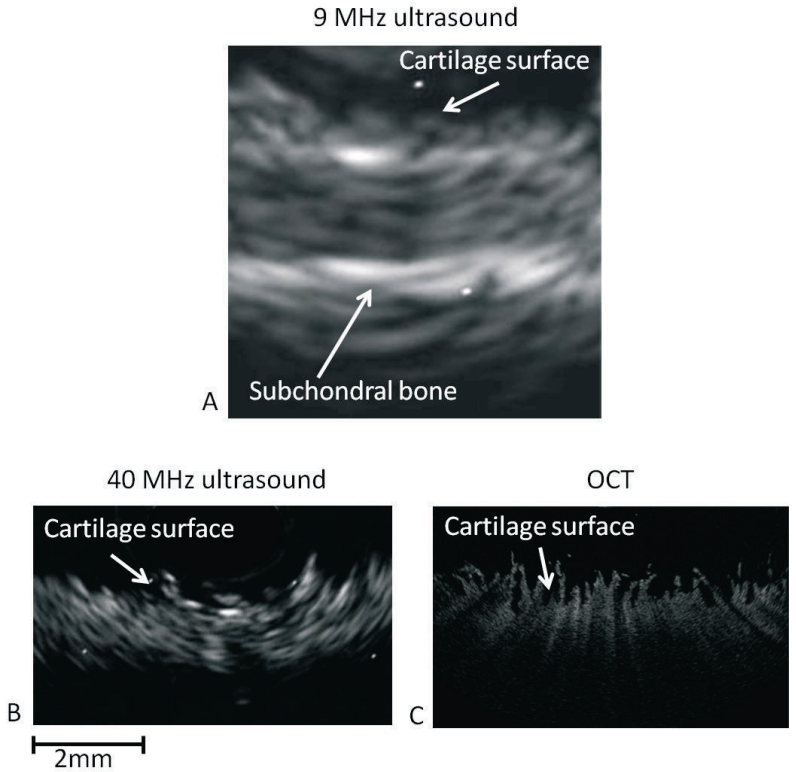

Figure 7.1: Representative ***A.*** *9 MHz ultrasound (Ultra Ice^{TM}, Boston Scientific Corporation, San Jose, CA, USA);* ***B.*** *40 MHz ultrasound;* ***C.*** *OCT (Lightlab imaging C7-XR^{TM} OCT Intravascular Imaging System, St. Jude Medical, Incorporation, St. Paul, USA) images of spontaneously degenerated human lateral tibia plateau cartilage and subchondral bone. The subchondral bone was visible only in the 9 MHz ultrasound image. The irregular cartilage surface was visible in all images. However, in the OCT images, the structure of the cartilage surface could be visualized with the greatest accuracy.*

in spontaneously healed tissue although statistical significance was not reached. The reproducibilities of ultrasound and optical parameters were either good or moderate (sCV = 1.4 % - 9.4 % and sCV = 5.0 % - 15.6 %, for ultrasound and OCT, respectively).

Table 7.2: Ultrasound reflection (R and IRC), roughness (URI) and backscattering (AIB) parameters (mean ± SD) as well as histological O'Driscoll grades for surgically and spontaneously repaired rabbit articular cartilage. The difference in R, IRC, AIB and URI values between the intact and surgically repaired tissues were statistically significant ($p < 0.05$). Furthermore the differences in URI values between the intact and spontaneously repaired tissue were statistically significant ($p < 0.05$). There were difference in R, IRC and AIB values between the intact and spontaneously repaired tissues but the changes were not statistically significant ($p = 0.08$). The histological grading showed that the surgically repaired tissue was similar to the spontaneously repaired tissue ($p = 0.41$) and that both repair groups were significantly inferior in structure, as compared to intact control tissue ($p < 0.05$). The O'Driscoll grading was obtained from a recent study of the same samples [132]. The intact control samples were not available for ultrasound measurements.

	R (%)	*IRC* (dB)	*URI* (μm)	*AIB* (dB)	O'Driscoll
Surgical repair					
Repair	7.0±1.9	-24.6±2.5	8.9±3.0	-46.0±2.9	12.5±1.8*◇
Adjacent tissue	1.7±1.0*	-39.9±2.5*	29.6±7.0*	-36.8±6.2*	
Spontaneous repair					
Repair	7.4±3.7	-24.8±6.5	7.9±4.0	-45.9±3.5	14.9±.6*
Adjacent tissue	2.0±1.3	-40.0±3.7	28.8±2.6*	-32.9±12.2	
Intact	-	-	-	-	29.1±0.9

*$p < 0.05$, non-parametric Wilcoxon signed rank test.
◇ The O'Driscoll score could be determined only for six samples because of the poor quality of some histological sections.

Significant correlations were detected between the ultrasound reflection or roughness and optical reflection or roughness parameters (Study III, Table 3 and Table 4). However, only a weak correlation was detected between the ultrasound and optical backscattering parameters.

The histological analysis revealed that the surgically repaired tissue was qualitatively similar with the spontaneously repaired tissue and that both repairs were significantly inferior to intact cartilage (Table 7.2). Furthermore, the histological images revealed that repaired tissue consisted of an abnormally organized collagen network, rough articular surface and there were low type II colla-

Table 7.3: Mean values and standard deviations of the integrated reflection coefficient (IRC), optical refection coefficient (ORC), ultrasound roughness index (URI), optical roughness index (ORI), apparent integrated backscattering (AIB) and optical backscattering (OBS) parameters for the spontaneously repaired and adjacent intact horse articular cartilage. The difference in the ORC, IRC, AIB, ORI and URI values between the intact and spontaneously healed tissues were statistically significant ($p < 0.01$). Difference in the OBS values between intact and spontaneously healed tissue were statistically significant only for 2 mm and 6 mm lesions.

		2 mm	4 mm	6 mm	8 mm
Adjacent tissue					
	IRC	-24.2±3.5	-25.0±4.3	-23.8±3.4	-24.3±3.7
	ORC	-19.1±1.4	-19.4±1.8	-19.6±2.0	-20.9±2.0
	URI	8.1±2.1	8.0±3.0	8.3±2.9	10.4±5.1
	ORI	2.3±0.5	2.6±0.7	2.6±0.4	3.2±1.9
	AIB	-51.5±2.5	-50.9±4.2	-48.8±4.6	-51.0±4.7
	OBS	-26.0±0.7	-26.0±1.2	-25.8±1.4	-25.3±2.0
Repair					
	IRC	-36.7±4.0*	-37.1±3.5*	-38.0±4.8*	-41.4±7.3*
	ORC	-28.1±4.3*	-28.7±4.0*	-30.4±2.5*	-30.5±3.0*
	URI	26.8±9.7*	27.5±13.6*	32.0±8.7*	45.2±16.5*
	ORI	13.2±6.5*	12.8±4.9*	21.7±8.7*	20.2±8.8*
	AIB	-45.7±6.3*	-42.2±5.1*	-42.1±6.0*	-44.0±4.8*
	OBS	-24.3±1.9*	-24.3±3.5	-23.8±1.3*	-23.8±2.3

*$p < 0.01$, the non-parametric Wilcoxon signed rank test

gen and proteoglycan contents (Figures 7.2 and 7.3). Importantly, quantitative ultrasound parameters revealed the abnormal surface roughness and internal collagen structure as the decreased values of *R* and *IRC* and increased values of *URI* and *AIB*. Furthermore, the poor integration of the repair with the surrounding tissue was clearly visible in the ultrasound images (Figure 7.2 and 7.3).

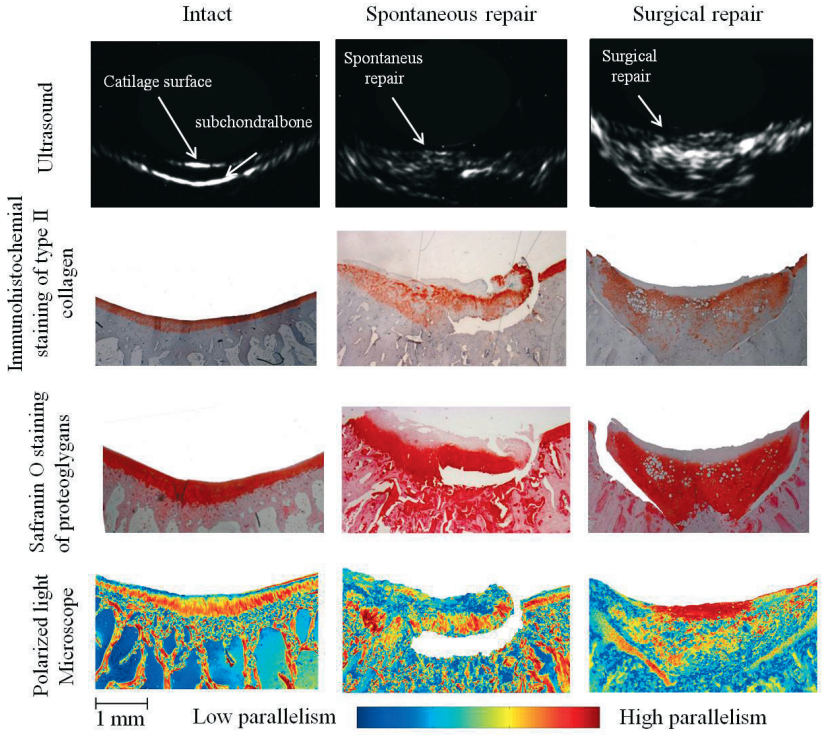

Figure 7.2: Representative ultrasound (top row), light microscope (Safranin O staining of proteoglycans and immunohistochemical staining of type II collagens, middle rows) and polarized light microscope (parallelism index [136], bottom row) images of intact, surgically repaired and spontaneously repaired rabbit articular cartilage samples. Increased roughness of the articular surface, low superficial collagen type II content and abnormal organisation of the collagen network, shown in the histological images of the repaired cartilage, can be diagnosed from the ultrasound images via the increased surface roughness, decreased surface reflection and higher echogeniaty of the internal cartilage.

Biomechanical measurements of the spontaneously healed horse cartilage indicated that the equilibrium and dynamic modulus val-

ues of repair tissue were lower than those of the intact cartilage ($p < 0.01$, $n = 44$). Interestingly, the dynamic and equilibrium modulus displayed significant correlations with the optical and ultrasound parameters (Table 4, see study III).

7.3 ULTRASOUND ARTHROSCOPY

In studies IV and V, the potential of the ultrasound arthroscopy technique was investigated under arthroscopic conditions *ex vivo* and *in vivo*, respectively.

Arthroscopic ultrasound imaging detected minor mechanical injuries artificially induced on cartilage surface of bovine knee (Table 7.4; Figure 2, see study IV). The Mankin scoring of the cartilage samples showed that the mechanically degraded tissue exhibited a low grade cartilage injury whereas the adjacent tissue was nearly normal (Table 7.4).

Table 7.4: The mean values and standard deviations of ultrasound (R, IRC, AIB and URI), light microscopic (RMS roughness) and mechanical parameters for intact and degraded cartilage in bovine femur and patella. The values of reflection and roughness parameters were lower and higher in mechanically degraded tissue, respectively. The AIB values determined for degraded and intact tissues were similar, indicating intact inner structure within the degraded cartilage. Indentation stiffness was slightly higher in adjacent intact than in degraded tissue, however the difference was not statistically significant.

	Femur		Patella	
	Intact	Degraded	Intact	Degraded
R (%)	4.1±1.3	2.0±0.9*	6.1±1.2	2.7±1.4*
IRC (dB)	-29.5±3.6	-36.0±4.1*	-25.4±1.9	-33.4±3.5*
AIB (dB)	-61.3±1.0	-61.2±0.9	-61.0±0.9	-61.1±1.5
URI (μm)	15.0±6.2	24.5±6.1*	10.7±3.6	25.6±14.9
Stiffness (N)	1.2±0.4	1.1±0.3	1.3±0.4	1.1±0.3
RMS roughness (μm)	6.7±1.8	11.5±4.3*	57.2±29.6	68.1±32.6*
Mankin Score	0.6±0.4	0.7±0.7	2.0±0.2	2.0±0.7*

*$p<0.05$, the non-parametric Wilcoxon signed rank test

The mark created to separate intact and degraded tissue was clearly visible in the ultrasound images (Figure 3, see study IV). Furthermore, a significant correlation ($r = 0.66$, $p = 0.001$ $p = 0.04$, p

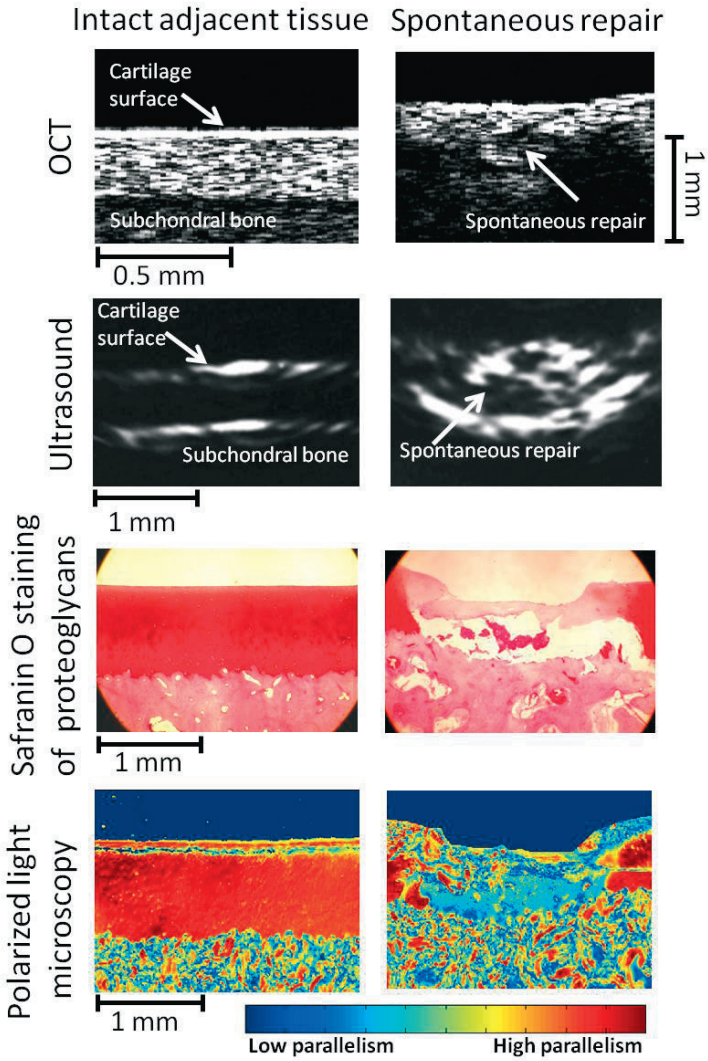

Figure 7.3: Representative ultrasound, OCT, light microscopy, and polarized light microscopy images of spontaneously repaired (lesion size 2 mm) and intact cartilage. Irregular surface, abnormal collagen orientation and abnormal collagen and proteoglycan contents evident in histological sections of repaired tissue can be visualized from the qualitative ultrasound and OCT images.

= 0.049) was found between the average depths of the mark separating the intact and control sites measured with ultrasound and from histological sections. In addition, the mean absolute values of cartilage thickness were in good agreement, being 0.75±0.2 mm and 0.73±0.25 mm, for ultrasound and light microscopy, respectively.

Indentation stiffness of intact cartilage revealed a slightly higher values, as compared to those of mechanically degraded tissue (Table 7.4). However, the difference was not statistically significant. Furthermore, significant linear correlations were revealed between the cartilage indentation stiffness and R or IRC in patellar tissue (r = 0.60, p = 0.02 and r = 0.67, p = 0.009, for R and IRC, respectively).

Human knee articular cartilage from seven patients was evaluated with the arthroscopic ultrasound technique during routine clinical arthroscopies (Figure 7.4). In some cases (*i.e*. Figure 7.4b.) the fibrillation of the cartilage surface was not visible in the arthroscopic image but could be visualised with ultrasound arthroscopy. Furthermore, the ultrasound reflection parameters calculated from the ultrasound signal were lower and URI was correspondigly higher, in fibrillated cartilage in comparison with intact cartilage (Figures 7.4a and 7.4b).

Full depth cartilage lesions were detected from ultrasound images by the increase of scattering inside the cartilage (Figures 7.4c). Thus, the ultrasound arthroscopy enabled evaluation of the cartilage inner structures which is not possible in conventional arthroscopy.

In some cases, the subchondral bone could be detected from ultrasound images and the cartilage thickness could be quantitatively measured (Figure 7.4). Importantly, the depth of the cartilage lesions relative to the cartilage thickness could be quantitatively measured (Figure 7.4d.). The depth of the lesion relative to the cartilage thickness was approximately 58 % (Figure 7.4d.).

A high correlation value (r = 0.939, p < 0.01) was found between the ultrasound score and ICRS score evaluated from thirteen cases by one of the operating surgeons. The ultrasound score differed from the ICRS score in total of four cases. In those four cases, the

ultrasound score was one rank higher than the ICRS grade indicating that the status of the cartilage in those cases was worse when assessed with the ultrasound arthroscopy than that estimated during conventional arthroscopy.

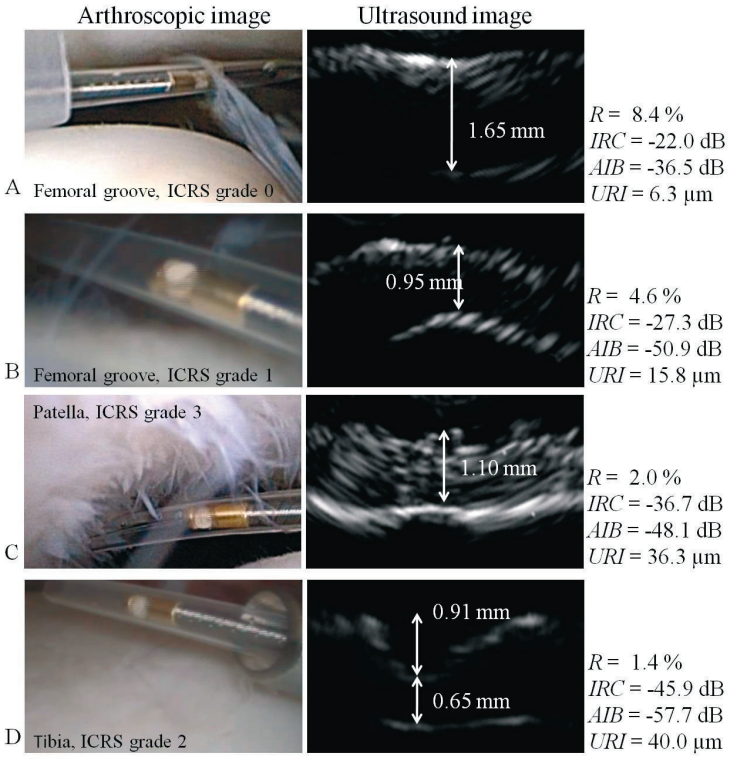

Figure 7.4: Arthroscopic and ultrasound images of articular cartilage in the human knee joints. The diameter of the ultrasound catheter (visible in the arthroscopic images) is 1 mm. The International Cartilage Repair Society (ICRS) grade assessed for each measurement site is shown on the arthroscopic images. In the ultrasound images, the direction of the incident ultrasonic signal is from the physiological saline (above) to the articular cartilage (below). The quantitative ultrasound parameters calculated using the ultrasonic signal are shown on the ultrasound images.

8 Discussion

In this thesis, a novel ultrasound technique to be used in the arthroscopic evaluation of the integrity of articular cartilage was introduced. In study I, the arthroscopic ultrasound technique was initially described and validated in the laboratory. Study II focused on assessing the potential of the ultrasound technique for evaluating the quality of surgical and spontaneous cartilage repair in rabbit samples *in vitro*. In study III, the potential of the ultrasound technique to evaluate the integrity of spontaneously repaired horse articular cartilage was compared to that of the OCT technique. In studies IV and V, the feasibility of using ultrasound arthroscopy was investigated with bovine knee joints *ex vivo* and clinically *in vivo*.

8.1 ULTRASONIC EVALUATION OF ARTIFICIALLY DEGRADED ARTICULAR CARTILAGE

In study I, the potential of the arthroscopic ultrasound technique was evaluated by conducting measurements with artificially degraded articular cartilage samples and non-biological phantoms with different surface characteristics. In line with earlier studies, the mechanical degradation of the cartilage surface decreased the ultrasound reflection and increased the ultrasound roughness index (URI) of the cartilage surface [2, 138]. Enzymatic digestion of the superficial collagen network decreased significantly ultrasound reflection amplitude emerging from the cartilage surface. This is also in line with earlier papers reporting similar results [116, 138, 153].

URI has been proposed to be a potential parameter for clinical use [77,138]. Unlike ultrasound parameters based on the quantification of ultrasound reflection and scattering, no reference measurements are needed in the determination of URI. Furthermore, values of URI might not be as sensitive as the reflection parameters to the

errors in the positioning of the ultrasound catheter (*i.e.* the angle between the ultrasound probe and the cartilage surface) which may be an advantage in clinical use [77]. However, due to the strong angular dependence of the ultrasound reflection at the cartilage surface, the length of the cartilage surface profile obtainable with the present rotating ultrasound probe is limited. In principle, this may limit the accuracy of detection of URI with the present ultrasound system. However, the reproducibilities of URI determined in this thesis were good to moderate (sCV = 3.7 - 7.9%). Furthermore, values of URI determined for intact bovine, rabbit and horse cartilage were similar to those determined in a previous studies for intact bovine cartilage using a linear scanning ultrasound system and ultrasound frequency of 20-50 MHz [77, 138]. Thus, despite the above mentioned limitations, the arthroscopic ultrasound system does possess the potential to detect changes in the roughness of articular surface.

Artificially degraded cartilage could be discerned from intact tissue by measurement of R or IRC. Basically, R and IRC quantify the same phenomena, *i.e.* the ultrasound power reflected from the cartilage surface. However, in the determination of IRC, a greater proportion of the collected data is used than in the determination of R and, thus, the values of IRC might be less sensitive to noise. On the other hand, determination of IRC requires considerably more computing resources and, therefore, R could be more feasible for clinical applications. According to the earlier studies [138, 139], no statistically significant difference has been observed between the reflection parameters R and IRC.

Emery paper phantoms were used to test the system's ability to detect differences in surface characteristics of a non-biological material. In general, the reflection coefficients decreased as the average particle size of the emery paper increased. The relationship between the reflection amplitude or surface roughness and average particle size of the emery paper was linear up to particle size of 120 μm. This is in line with an earlier study in which a strong linear correlation was found between the ultrasound parameter values

and particle size of the emery paper [163].

8.2 ULTRASONIC AND OCT EVALUATION OF REPAIRED ARTICULAR CARTILAGE

The ultrasound arthroscopy technique was capable of detecting changes in the structure and composition of surgically and spontaneously repaired cartilage (Studies II and III). Surface roughness (URI) was significantly higher in surgically and spontaneously repaired tissue than in intact cartilage. Similar results have been reported in earlier studies [57,90]. Furthermore, in line with previous studies, the values of the reflection parameters measured from the repair sites were lower than those measured for intact cartilage [64,90].

The values of AIB were significantly higher for repaired cartilage as compared to intact cartilage. Since collagen is the main scatterer of ultrasound in soft tissues [153], an increase in AIB is speculated as representing abnormalities in the organization and composition of the collagen network. This was supported by the polarized light microscopy in which the abnormal collagen orientation in the cartilage repair could be visualized. These results are in line with an earlier report in which AIB was found to detect age-related changes in the amount and orientation of the collagen network [30]. Furthermore, in the recent study of Gelse *et al*. [49] the slope of AIB with respect to the distance to the cartilage surface was related to the integrity of the repaired tissue.

The ultrasound findings were supported by the histological grading (O'Driscoll) which showed that the surgically repaired tissue was structurally similar to the spontaneously repaired tissue [132] and that the repaired tissues exhibited impaired histological structure, as compared with intact tissue [132]. Furthermore, both repair groups (rabbit and horse) displayed rough and irregular cartilage surface, abnormal collagen structures as well as poor integration of the repair tissue with the surrounding tissues. Importantly, this same information could also be extracted from the qualitative ultrasound images. Since conventional arthroscopy enables only in-

vestigation of the integrity of cartilage surface, ultrasound might provide important information about the integrity of inner structures of the cartilage repair.

The spontaneously healed horse cartilage lesions could be distinguished from intact adjacent tissue by both ultrasound and OCT techniques (Study III). The reflection parameters were higher at the surface of intact tissue as compared with the spontaneously repaired tissue. Similar results have been reported in earlier studies in which spontaneously repaired cartilage was studied with ultrasound or OCT [57, 90]. The rough and irregular surface of regenerated cartilage could be quantified with both techniques. Surface roughness of intact tissue was significantly lower than that of repaired cartilage. This result is in agreement with a published report in which rabbit cartilage was investigated with OCT [57].

Similar to study II, the values of *AIB* determined in study III were significantly higher for all repaired horse cartilage lesions in comparison to those from intact cartilage. *OBS* was higher for repaired cartilage than for intact cartilage. However, the difference in *OBS* values was statistically significant only for 2 mm and 6 mm lesions. Histology confirmed that all lesions exhibited an abnormal collagen structure. The dynamic and equilibrium moduli correlated with the optical or ultrasound reflection and roughness parameters. In earlier studies, cartilage dynamic and equilibrium moduli have been reported to correlate with the ultrasound reflection amplitude [140]. However, it should be noted that the ultrasound reflection is not a direct measure of cartilage stiffness, but the correlation is most probably secondary.

8.3 COMPARISON OF ULTRASOUND AND OCT TECHNIQUES IN EVALUATION OF HORSE ARTICULAR CARTILAGE

Both ultrasound and the OCT application were capable of detecting the abnormal structure and composition of spontaneously repaired horse cartilage. Significant correlations were detected between the

ultrasound and the optical reflection or roughness parameters. Furthermore, significant correlations were detected between reflection and roughness parameters. These findings are consistent with earlier studies indicating that the integrity of the cartilage superficial collagen network and surface roughness are the two major components controlling the ultrasound reflection from the cartilage surface [138, 141, 153]. The values of ORI were systematically lower than values of URI. This is most probably due to the higher resolution of the OCT device which enabled a more accurate determination of the distance between the cartilage surface and the probe as well as to differences in the measurement geometries (linear scanning vs. rotating probe). However, the differences in both surface roughness parameters (ORI and URI) between the intact and repaired tissue were statistically significant. The reproducibilities of the ultrasound and optical parameters ranged from good to moderate. However, reproducibilities of ultrasound parameters were slightly better than those of the OCT parameters.

With current ultrasound and OCT devices the ultrasound seems to be more sensitive for assessing changes in the content and orientation of the cartilage inner collagen network. However, the light scattering from the inner structures of cartilage is more complicated than that from ultrasound scattering and, thus, for reliable quantification of the integrity of the cartilage inner structures, more complex attenuation corrections should be used with OCT. Furthermore, the signal-to-noise ratio of the current OCT device was relatively low which could explain its lower sensitivity to differences in the internal structure of the tissue. With more sophisticated, *e.g.*, polarization sensitive OCT devices, more detailed information on the integrity of the cartilage inner structures may be obtained.

The capability to estimate the structure, density and composition of subchondral bone would be of clinical value. Unfortunately, the attenuation of sound and light with the present devices was too intensive to acheive a reliable evaluation of the subchondral bone. The quantitative imaging of subchondral bone can be conducted by using a lower ultrasound frequency. However, the use of lower

ultrasound frequencies diminishes the axial resolution, which decreases also the accuracy of the URI and sensitivity of AIB [77]. One possible solution could be a catheter combining the ultrasound and OCT modalities as proposed by Yin et al. [166]. This integrated imaging modality with an ultrasound frequency low enough could enable simultaneous imaging of the cartilage surface and subchondral bone with the best possible resolution. Another possibility could be a catheter with multiple ultrasound transducers of different center frequencies or, alternatively, with one broadband ultrasound transducer enabling the use of a wide spectrum of ultrasound frequencies.

8.4 ULTRASOUND ARTHROSCOPY

Ultrasound arthroscopy was found to be applicable for the evaluation of the integrity of articular cartilage *ex vivo* and *in vivo* (Studies IV and V). The mechanically degraded bovine knee cartilage could be discerned from intact adjacent tissue in arthroscopic conditions *ex vivo* (Study IV). Ultrasound roughness index was higher in mechanically degraded tissue than in intact adjacent tissue. Furthermore, the ultrasound reflection parameters were lower in degraded tissue than in intact cartilage. Similar results have been reported in earlier *in vitro* studies [77,138]. A significant correlation was found between the parameters measuring the cartilage surface reflection and indentation stiffness in patellar cartilage. Furthermore, a significant correlation was found between URI and RMS roughness of the cartilage surface measured from light microscopy images. The absolute values of RMS roughness were systematically lower than those of URI. Furthermore, the present values of URI measured from intact tissue were slightly higher than those in a previous study where bovine knee cartilage was investigated *in vitro* with the same ultrasound instrumentation [156]. A possible error in the positioning of the ultrasound transducer in arthroscopic conditions might explain the higher URI values measured in the present study.

The values of AIB were similar to intact and mechanically de-

graded tissue indicating that the mechanical degradation extended only to the superficial layers of the cartilage (Study IV). This was also confirmed in the histological analysis. *AIB* could be valuable in clinical use as the conventional arthroscopic examination enables only the evaluation of the integrity of cartilage surface. Furthermore, as *AIB* is based on the measurement of ultrasound scattering, it might not be highly dependent on the positioning of the ultrasound transducer, *i.e.*, the angle between the ultrasound transducer and cartilage surface, which would be advantageous in clinical use.

With the arthroscopic ultrasound technique, various conditions of the human articular cartilage could be detected and evaluated during clinical arthroscopy *in vivo* (Study V). Superficial fibrillation, not always detectable with an arthroscope, could be measured by ultrasound. This finding is in line with earlier studies indicating that micrometer scale fibrillation can be detected with ultrasound [138]. Furthermore, almost intact cartilage (ICRS grade 1) could be discerned from intact tissue (ICRS grade 0) quantitatively with ultrasound parameters and qualitatively from the ultrasound image.

Imaging of subchondral bone and the measurement of cartilage thickness are essential if one wishes to evaluate the integrity of articular cartilage. The present ultrasound device could be used to measure cartilage thickness during clinical arthroscopy. However, due to the strong attenuation of ultrasound in cartilage, the tissue thickness could be measured only in the case of thin cartilage (thickness < 2 mm). In a recent study, the thickness of cartilage at human lateral tibial plateau could be measured with a 9 MHz ultrasound catheter (unpublished). Furthermore, the scattering from subchondral bone inner structure could be visualized. Since information on cartilage thickness and the status of subchondral bone is diagnostically valuable, the use of 9 MHz catheters could be justified.

Accurate measurements of size and extent of cartilage lesions are essential in several cartilage scoring systems (*e.g.* ICRS scoring). Currently, the evaluation of the extent of cartilage lesion is challenging if one uses only a conventional arthroscopy [112]. With

ultrasound, the depth of the cartilage lesion could be accurately measured during arthroscopy *in situ* (Study IV). Importantly, the depth of the cartilage lesion relative to the cartilage thickness could be evaluated also during clinical arthroscopy (Study, V). The ultrasound investigation affected significantly to the arthroscopic evaluation of the severity of cartilage injuries. In 4 cases out of 13, the ultrasound findings indicated more severe cartilage injury than the ICRS grade. In the remaining 9 cases, the ultrasound score value was similar to the ICRS score value. These results indicate that the ultrasound investigation could provide more information than the conventional arthroscopy about the integrity of the articular cartilage.

The reproducibilities of the ultrasound parameters in an arthroscopic examination were variable (study IV). This is most probably due to the variation in positioning (*i.e*. the angle between the ultrasound transducer and cartilage surface) of the ultrasound catheter during the repeated measurements. However, because of the large difference in the values of ultrasound parameters between intact and degenerated, injured or repaired cartilage, a reliable detection of degrated or injured cartilage might be possible despite the variable reproducibility. Furthermore, the development of the arthroscopic tools and procedures that enable more accurate positioning of the ultrasound transducer might improve the reproducibility of the arthroscopic ultrasound measurements and enhance their diagnostic sensitivity.

8.5 CHALLENGES TO CLINICAL APPLICATION

Despite the current encouraging results, there are still several limitations and challenges related to the clinical application of the arthroscopic ultrasound technique that need to be discussed.

Since the ultrasound examination of the joint has to be conducted during arthroscopy, the usability of arthroscopic ultrasound technique for diagnosis and screening of OA is limited. Furthermore, because of the lack of effective treatments for OA, the ad-

vantage of ultrasound investigations may be debated. However, as arthroscopy, is a routine procedure for evaluation of the extent and severity cartilage lesions, the quantitative ultrasound measurements could have diagnostic value. In fact, in a recent study, the majority (78%) of experienced arthroscopists considered some quantitative measurement tool would be valuable to help in the determination of the integrity of articular cartilage [147]. Furthermore, the development of cartilage repair treatments would benefit from an accurate estimate of the lesion for planing of the surgery and more sensitive monitoring of the healing of the tissue and outcome of the treatment. It has been also stated that accurate quantitative imaging methods are needed also for developing medical treatments for OA [133].

The quantitative ultrasound parameters are highly dependent on the angle between the ultrasound transducer and cartilage surface [77]. In the direction parallel to the long axis of the ultrasound catheter, the angle between the ultrasound probe and the cartilage surface must be adjusted manually to achieve the maximum reflection. This is both challenging and time consuming under clinical conditions and, thus, may jeopardize the quantitative measurements. Furthermore, the curvature of the articular surfaces, for example in the knee joint, may limit the areas that can be reliably imaged with the arthroscopic ultrasound technique. However, because the technique is based on the use of a flexible ultrasound catheter, arthroscopic tools of different shapes might be used to access different areas within the joint. However, further development of arthroscopic tools would be needed to achieve more reproducible and straightforward positioning of the ultrasound catheter.

Current ultrasound catheters are designed for intravascular imaging and, thus, may not be optimal for arthroscopic use. Due to the fragile and disposable design of the catheters, the high cost of ultrasound investigations may limit the clinical use of the current catheters. Furthermore, the frequency of the ultrasound transducer should be optimized for imaging of articular cartilage and subchondral bone. The 40 MHz transducer used in present study does en-

able high resolution imaging of the cartilage surface layer. However, the evaluation of the cartilage thickness, the status of the cartilage inner structure and subchondral bone might increase the value of the ultrasound investigation and thus, lower frequency ultrasound transducers might be more optimal for arthroscopic use. However, the lower resolution which is inherent in the low frequency ultrasound transducers might decrease the diagnostic power of ultrasound investigation and decrease the advantages of the ultrasound as compared with, for example, clinical MRI.

9 Conclusions

In this study a new ultrasound technique was introduced for arthroscopic evaluation of the articular cartilage. The arthroscopic ultrasound technique possessed significant potential for use in the evaluation of the integrity of articular cartilage and cartilage repair in laboratory as well as during clinical arthroscopies. The main results and conclusions of the thesis can be summarised as follows:

1. With the arthroscopic ultrasound technique the mechanical and enzymatical degradation of an articular surface could be diagnosed. Furthermore, different surface characteristics of non-biological phantoms could be distinguished with the technique.

2. Surface roughness and the integrity of the intact and surgically repaired cartilage could be quantitatively evaluated with the ultrasound technique. Furthermore, qualitative information on the integration of the repair tissue, the integrity of the surface and the internal structure of repair tissue could be extracted from the ultrasound images.

3. The applied ultrasound and OCT techniques could differentiate the spontaneously repaired cartilage from the intact tissue. The superior resolution of OCT enabled more reliable measurements of cartilage surface integrity, but with ultrasound, more information was obtained from the inner structures of the tissue. Both techniques were incapable of visualizing subchondral bone and, thus, novel dual modality OCT and ultrasound or broadband ultrasound imaging techniques are needed to achieve simultaneous high resolution imaging of cartilage and subchondral bone.

4. Mechanically degraded cartilage could be quantitatively distinguished from intact tissue under arthroscopic control *ex vivo*. Furthermore, a cartilage injury could be diagnosed and the depth of cartilage lesion could be measured from the ultrasound images. However, the development of customized arthroscopic tools will be required for more reproducible and straigthforward measurements.

5. The arthroscopic ultrasound technique was feasible for inclusion into clinical arthroscopy *in vivo* and provided valuable diagnostic information about the integrity and thickness of the cartilage not available in conventional arthroscopy.

To conclude, the arthroscopic ultrasound technique enabled the evaluation of the integrity of articular cartilage both *in vitro* and *in vivo*. However, the imaging of subchondral bone and measurement of cartilage thickness were not always possible. For this reason, application of broadband ultrasound catheters could be better suited for the clinical application of the arthroscopic ultrasound technique.

Bibliography

[1] A. Adam and A. J. Spence, "Intertrocnanteric osteotomy for osteoarthritis of the hip; a review of fifty-eight operations," *J Bone Joint Surg Br* **40-B,** 219–26 (1958).

[2] R. S. Adler, D. K. Dedrick, T. J. Laing, E. H. Chiang, C. R. Meyer, P. H. Bland, and J. M. Rubin, "Quantitative assessment of cartilage surface roughness in osteoarthritis using high frequency ultrasound," *Ultrasound Med Biol* **18,** 51–8 (1992).

[3] D. H. Agemura, J. O'Brien, W. D., J. E. Olerud, L. E. Chun, and D. E. Eyre, "Ultrasonic propagation properties of articular cartilage at 100 MHz," *J Acoust Soc Am* **87,** 1786–91 (1990).

[4] R. C. Appleyard, M. V. Swain, S. Khanna, and G. A. Murrell, "The accuracy and reliability of a novel handheld dynamic indentation probe for analysing articular cartilage," *Phys. Med. Biol.* **46,** 541–50. (2001).

[5] N. Arden and M. C. Nevitt, "Osteoarthritis: epidemiology," *Best Pract Res Clin Rheumatol* **20,** 3–25 (2006).

[6] C. G. Armstrong and V. C. Mow, "Variations in the intrinsic mechanical properties of human articular cartilage with age, degeneration, and water content," *J Bone Joint Surg Am* **64,** 88–94 (1982).

[7] R. M. Aspden and D. W. Hukins, "Collagen organization in articular cartilage, determined by X-ray diffraction, and its relationship to tissue function," *Proc R Soc Lond B Biol Sci* **212,** 299–304 (1981).

[8] G. A. Ateshian, "The role of interstitial fluid pressurization in articular cartilage lubrication," *J Biomech* **42,** 1163–1176 (2009).

[9] A. Bashir, M. L. Gray, and D. Burstein, "Gd-DTPA2- as a measure of cartilage degradation," *Magn Reson Med* **36,** 665–73 (1996).

[10] A. Bashir, M. L. Gray, J. Hartke, and D. Burstein, "Nondestructive imaging of human cartilage glycosaminoglycan concentration by MRI," *Magn Reson Med* **41,** 857–65 (1999).

[11] A. Bedi, B. T. Feeley, and r. Williams, R. J., "Management of articular cartilage defects of the knee," *J Bone Joint Surg Am* **92,** 994–1009 (2010).

[12] G. Bentley, L. C. Biant, R. W. Carrington, M. Akmal, A. Goldberg, A. M. Williams, J. A. Skinner, and J. Pringle, "A prospective, randomised comparison of autologous chondrocyte implantation versus mosaicplasty for osteochondral defects in the knee," *J Bone Joint Surg Br* **85,** 223–30 (2003).

[13] I. Bjarnason, J. Hayllar, A. J. MacPherson, and A. S. Russell, "Side effects of nonsteroidal anti-inflammatory drugs on the small and large intestine in humans," *Gastroenterology* **104,** 1832–47 (1993).

[14] G. M. Blake, H. W. Wahner, and I. Fogelman, *The evaluation of osteoporosis: Dual energy X-ray absorptiometry and ultrasound in clinical practice*, 2nd edition ed. (Martin Dunitz Ltd, London, 1999).

[15] J. Borrelli, J., M. J. Silva, M. A. Zaegel, C. Franz, and L. J. Sandell, "Single high-energy impact load causes posttraumatic OA in young rabbits via a decrease in cellular metabolism," *J Orthop Res* **27,** 347–52 (2009).

[16] H. A. Breinan, S. D. Martin, H. P. Hsu, and M. Spector, "Healing of canine articular cartilage defects treated with microfracture, a type-II collagen matrix, or cultured autologous chondrocytes," *J Orthop Res* **18,** 781–9 (2000).

[17] M. Brittberg, E. Faxen, and L. Peterson, "Carbon fiber scaffolds in the treatment of early knee osteoarthritis. A prospective 4-year followup of 37 patients," *Clinical Orthopaedics Related Research* 155-64 (1994).

[18] M. Brittberg and C. S. Winalski, "Evaluation of cartilage injuries and repair," *J Bone Joint Surg Am* **85-A Suppl 2,** 58–69 (2003).

[19] J. A. Buckwalter and S. Lohmander, "Operative treatment of osteoarthrosis. Current practice and future development," *J Bone Joint Surg Am* **76,** 1405–18 (1994).

[20] J. A. Buckwalter and J. Mankin, "Articular cartilage: Part II. Degeneration and osteoarthritis, repair, regeneration, and transplantation," *J Bone Joint Surg Am* **79-A,** 612–632 (1997).

[21] J. A. Buckwalter and J. Martin, "Degenerative joint disease," *Clin Symp* **47,** 1–32 (1995).

[22] J. A. Buckwalter and J. A. Martin, "Osteoarthritis," *Adv Drug Deliv Rev* **58,** 150–167 (2006).

[23] J. A. Buckwalter, L. C. Rosenberg, and E. B. Hunziker, "Articular cartilage: Composition, structure, response to injury, and methods of facilitating repair," in *Articular cartilage and knee joint function: Basic science and arthroscopy.*, J. W. Ewing, ed. (Raven Press Ltd., New York, 1990), pp. 19-56.

[24] W. D. Bugbee and F. R. Convery, "Osteochondral allograft transplantation," *Clin Sports Med* **18,** 67–75 (1999).

[25] P. S. Burrage and C. E. Brinckerhoff, "Molecular targets in osteoarthritis: metalloproteinases and their inhibitors," *Curr Drug Targets* **8,** 293–303 (2007).

[26] R. E. Challis and R. I. Kitney, "Biomedical signal processing (in four parts). Part 1. Time-domain methods," *Med Biol Eng Comput* **28,** 509–24 (1990).

[27] W. Cheong, S. A. Prahl, and A. J. Welch, "A refiew of the optical properties of biological tissues," *IEEE Jour. Quant. Electron.* **26,** 2166–2185 (1990).

[28] E. H. Chiang, R. S. Adler, C. R. Meyer, J. M. Rubin, D. K. Dedrick, and T. J. Laing, "Quantitative assessment of surface roughness using backscattered ultrasound: the effects of finite surface curvature," *Ultrasound Med Biol* **20,** 123–135 (1994).

[29] E. Chérin, A. Saïed, P. Laugier, P. Netter, and G. Berger, "Evaluation of acoustical parameter sensitivity to age-related and osteoarthritic changes in articular cartilage using 50-MHz ultrasound," *Ultrasound Med Biol* **24,** 341–354 (1998).

[30] E. Chérin, A. Saïed, B. Pellaumail, D. Loeuille, P. Laugier, P. Gillet, P. Netter, and G. Berger, "Assessment of rat articular cartilage maturation using 50-MHz quantitative ultrasonography," *Osteoarthritis Cartilage* **9,** 178–186 (2001).

[31] C. R. Chu, F. R. Convery, W. H. Akeson, M. Meyers, and D. Amiel, "Articular cartilage transplantation. Clinical results in the knee," *Clinical Orthopaedics Related Research* 159-68 (1999).

[32] C. R. Chu, N. J. Izzo, J. J. Irrgang, M. Ferretti, and R. K. Studer, "Clinical diagnosis of potentially treatable early articular cartilage degeneration using optical coherence tomography," *J Biomed Opt* **12,** 051703 (2007).

[33] C. R. Chu, D. Lin, J. L. Geisler, C. T. Chu, F. H. Fu, and Y. Pan, "Arthroscopic microscopy of articular cartilage using optical coherence tomography," *Am J Sports Med* **32,** 699–709 (2004).

[34] P. A. Davidson, D. W. Rivenburgh, P. E. Dawson, and R. Rozin, "Clinical, histologic, and radiographic outcomes of distal femoral resurfacing with hypothermically stored osteoarticular allografts," *Am J Sports Med* **35,** 1082–90 (2007).

[35] D. G. Disler, E. Raymond, D. A. May, J. S. Wayne, and T. R. McCauley, "Articular cartilage defects: in vitro evaluation of accuracy and interobserver reliability for detection and grading with US," *Radiology* **215,** 846–851 (2000).

[36] F. A. Duck, A. C. Baker, and H. C. Starritt, *Ultrasound in medicine* (IOP publishing Ltd, Bristol, 1998).

[37] T. C. Dunn, Y. Lu, H. Jin, M. D. Ries, and S. Majumdar, "T2 relaxation time of cartilage at MR imaging: comparison with severity of knee osteoarthritis," *Radiology* **232,** 592–8 (2004).

[38] F. Eckstein, H. Sittek, S. Milz, R. Putz, and M. Reiser, "The morphology of articular cartilage assessed by magnetic resonance imaging (MRI). Reproducibility and anatomical correlation," *Surg Radiol Anat* **16,** 429–38 (1994).

[39] M. J. Elders, "The increasing impact of arthritis on public health," *J Rheumatol Suppl* **60,** 6–8 (2000).

[40] W. F. Enneking and D. A. Campanacci, "Retrieved human allografts : a clinicopathological study," *J Bone Joint Surg Am* **83-A,** 971–86 (2001).

[41] D. T. Felson, "Obesity and knee Osteoarthritis," *ann Intern Med* **109,** 18–24 (1988).

[42] D. T. Felson, "Preventing knee and hip osteoarthritis," *Bull Rheum Dis* **47,** 1–4 (1998).

[43] D. T. Felson, R. C. Lawrence, P. A. Dieppe, R. Hirsch, C. G. Helmick, J. M. Jordan, R. S. Kington, N. E. Lane, M. C. Nevitt, Y. Zhang, M. Sowers, T. McAlindon, T. D. Spector, A. R. Poole, S. Z. Yanovski, G. Ateshian, L. Sharma, J. A. Buckwalter, K. D. Brandt, and J. F. Fries, "Osteoarthritis: new insights. Part 1: the disease and its risk factors," *Ann Intern Med* **133,** 635–46 (2000).

[44] D. T. Felson and E. L. Radin, "What causes knee osteoarthrosis: are different compartments susceptible to different risk factors?," *J Rheumatol* **21,** 181–3 (1994).

[45] D. T. Felson, Y. Zhang, M. T. Hannan, A. Naimark, B. N. Weissman, P. Aliabadi, and D. Levy, "The incidence and natural history of knee osteoarthritis in the elderly," *Arthritis Rheumatism* **38,** 1500–1505 (1995).

[46] A. F. Fercher, W. Drexler, C. K. Hitzenberger, and T. Lasser, "Optical coherence tomography - principles and applications," *Rep. Prog. Phys* **66,** 239–303 (2003).

[47] P. J. Fitzgerald, F. G. St Goar, A. J. Connolly, F. J. Pinto, M. E. Billingham, R. L. Popp, and P. G. Yock, "Intravascular ultrasound imaging of coronary arteries. Is three layers the norm?," *Circulation* **86,** 154–8 (1992).

[48] J. G. Fujimoto, "Optical coherence tomography for ultrahigh resolution in vivo imaging," *Nat Biotechnol* **21,** 1361–7 (2003).

[49] K. Gelse, A. Olk, S. Eichhorn, B. Swoboda, M. Schoene, and K. Raum, "Quantitative ultrasound biomicroscopy for the analysis of healthy and repair cartilage tissue," *Eur Cell Mater* **19,** 58–71 (2010).

[50] N. Gerwin, C. Hops, and A. Lucke, "Intraarticular drug delivery in osteoarthritis," *Adv Drug Deliv Rev* **58,** 226–42 (2006).

[51] F. N. Ghadially, "Structure and function of articular cartilage," *Clin Rheum Dis* **7,** 3–28 (1981).

[52] M. T. Ghazavi, K. P. Pritzker, A. M. Davis, and A. E. Gross, "Fresh osteochondral allografts for post-traumatic osteochondral defects of the knee," *J Bone Joint Surg Br* **79,** 1008–13 (1997).

[53] P. D. Gikas, W. J. Aston, and T. W. Briggs, "Autologous chondrocyte implantation: where do we stand now?," *J Orthop Sci* **13,** 283–92 (2008).

[54] C. C. Glüer, G. Blake, Y. Lu, B. A. Blunt, M. Jergas, and H. K. Genant, "Accurate assessment of precision errors: how to measure the reproducibility of bone densitometry techniques," *Osteoporos Int* **5,** 262–70 (1995).

[55] V. M. Goldberg and J. A. Buckwalter, "Hyaluronans in the treatment of osteoarthritis of the knee: evidence for disease-modifying activity," *Osteoarthritis Cartilage* **13,** 216–24 (2005).

[56] E. J. Gussenhoven, C. E. Essed, P. Frietman, F. van Egmond, C. T. Lancee, W. H. van Kappellen, J. Roelandt, P. W. Serruys, G. P. Gerritsen, H. van Urk, and et al., "Intravascular ultrasonic imaging: histologic and echographic correlation," *Eur J Vasc Surg* **3,** 571–6 (1989).

[57] C. W. Han, C. R. Chu, N. Adachi, A. Usas, F. H. Fu, J. Huard, and Y. Pan, "Analysis of rabbit articular cartilage repair after chondrocyte implantation using optical coherence tomography," *Osteoarthritis Cartilage* **11,** 111–21 (2003).

[58] L. Hangody, G. Kish, Z. Karpati, I. Szerb, and I. Udvarhelyi, "Arthroscopic autogenous osteochondral mosaicplasty for the treatment of femoral condylar articular defects. A preliminary report," *Knee Surg Sports Traumatol Arthrosc* **5,** 262–7 (1997).

[59] G. Harris, "Review of transient field theory for a baffled planar piston," *J Acoust Soc Am* **70,** 10–20 (1981).

[60] W. H. Harris, "Etiology of osteoarthritis of the hip," *Clin Orthop* 20-33 (1986).

[61] K. Hattori, K. Ikeuchi, Y. Morita, and Y. Takakura, "Quantitative ultrasonic assessment for detecting microscopic cartilage damage in osteoarthritis," *Arthritis Res Ther* **7,** R38–R46 (2004).

[62] K. Hattori, Y. Takakura, M. Ishimura, T. Habata, K. Uematsu, and K. Ikeuchi, "Quantitative arthroscopic ultrasound evaluation of living human cartilage," *Clin Biomech* **19,** 213–216 (2004).

[63] K. Hattori, Y. Takakura, M. Ishimura, Y. Tanaka, T. Habata, and K. Ikeuchi, "Differential Acoustic Properties of Early Cartilage Lesions in Living Human Knee and Ankle Joints," *Arthritis Rheum* **52,** 3125–3131 (2005).

[64] K. Hattori, Y. Takakura, Y. Morita, M. Takenaka, K. Uematsu, and K. Ikeuchi, "Can ultrasound predict histological findings in regenerated cartilage?," *Rheumatology* **43,** 302–305 (2004).

[65] W. C. Hayes, L. M. Keer, G. Herrmann, and L. F. Mockros, "A mathematical analysis for indentation tests of articular cartilage," *J Biomech* **5,** 541–51 (1972).

[66] J. M. Herrmann, C. Pitris, B. E. Bouma, S. A. Boppart, C. A. Jesser, D. L. Stamper, J. G. Fujimoto, and M. E. Brezinski, "High resolution imaging of normal and osteoarthritic cartilage with optical coherence tomography," *J Rheumatol* **26,** 627–35 (1999).

[67] Y. P. Huang, S. Saarakkala, J. Töyräs, L. K. Wang, J. S. Jurvelin, and Y. P. Zheng, "Effects of optical beam angle on quantitative optical coherence tomography (OCT) in normal and surface degenerated bovine articular cartilage.," *Physics in Medicine and Biology* **in press** (2010).

[68] Y.-P. Huang and Y. P. Zheng, "Intravascular ultrasound (IVUS): a potential arthroscopic tool for quantitative assessment of articular cartilage," *Open Biomed Eng J* **3,** 13–20 (2009).

[69] E. B. Hunziker, "Articular cartilage repair: are the intrinsic biological constraints undermining this process insuperable? [Review]," *Osteoarthritis Cartilage* **7,** 15–28 (1999).

[70] J. N. Insall, D. M. Joseph, and C. Msika, "High tibial osteotomy for varus gonarthrosis. A long-term follow-up study," *J Bone Joint Surg Am* **66,** 1040–8 (1984).

[71] M. Insana, R. Wagner, D. Brown, and T. Hall, "Describing small-scale structure in random media using pulse-echo ultrasound," *J Acoust Soc Am* **87,** 179–192 (1990).

[72] G. D. Jay, J. R. Torres, M. L. Warman, M. C. Laderer, and K. S. Breuer, "The role of lubricin in the mechanical behavior of synovial fluid," *Proc Natl Acad Sci USA* **104,** 6194–6199 (2007).

[73] J. A. Jensen and N. B. Svendsen, "Calculation of pressure fileds from arbitarily shaped, apodized and excited ultrasound trasducers," *IEEE Trans Ultrason Ferroelectr Freq Control* **39,** 262–267 (1992).

[74] G. A. Joiner, E. R. Bogoch, K. P. Pritzker, M. D. Buschmann, A. Chevrier, and F. S. Foster, "High frequency acoustic parameters of human and bovine articular cartilage following experimentally-induced matrix degradation," *Ultrason Imaging* **23,** 106–116 (2001).

[75] J. Jurvelin, I. Kiviranta, A. M. Säämänen, M. Tammi, and H. J. Helminen, "Indentation stiffness of young canine knee articular cartilage– influence of strenuous joint loading," *J Biomech* **23,** 1239–46 (1990).

[76] J. Jurvelin, T. Kuusela, R. Heikkila, A. Pelttari, I. Kiviranta, M. Tammi, and H. J. Helminen, "Investigation of articular cartilage surface morphology with a semiquantitative scanning electron microscopic method," *Acta Anat* **116,** 302–311 (1983).

[77] E. Kaleva, S. Saarakkala, J. Jurvelin, T. Virén, and J. Töyräs, "Effects of ultrasound beam angle and surface roughness on the quantitative ultrasound parameters of articular cartilage," *Ultrasound Med Biol* **35,** 1344–1351 (2009).

[78] E. Kaleva, J. Töyräs, J. Jurvelin, T. Virén, and S. Saarakkala, "Effects of ultrasound frequency, temporal sampling frequency and spatial sampling step on the quantitative ultrasound parameters of articular cartilage," *IEEE Trans Ultrason Ferroelectr Freq Control* **56,** 1383–1393 (2009).

[79] M. A. Karsdal, D. J. Leeming, E. B. Dam, K. Henriksen, P. Alexandersen, P. Pastoureau, R. D. Altman, and C. Christiansen, "Should subchondral bone turnover be targeted when treating osteoarthritis?," *Osteoarthritis Cartilage* **16,** 638–46 (2008).

[80] J. N. Katz, "Total joint replacement in osteoarthritis," *Best Pract Res Clin Rheumatol* **20,** 145–53 (2006).

[81] H. K. Kim, M. E. Moran, and R. B. Salter, "The potential for regeneration of articular cartilage in defects created by chondral shaving and subchondral abrasion. An experimental investigation in rabbits," *J Bone Joint Surg Am* **73,** 1301–15 (1991).

[82] G. Kish and L. Hangody, "A prospective, randomised comparison of autologous chondrocyte implantation versus mosaicplasty for osteochondral defects in the knee," *J Bone Joint Surg Br* **86,** 619; author reply 619–20 (2004).

[83] N. B. Kock, J. L. Van Susante, P. Buma, A. Van Kampen, and N. Verdonschot, "Press-fit stability of an osteochondral autograft: Influence of different plug length and perfect depth alignment," *Acta Orthop* **77,** 422–8 (2006).

[84] G. Kordas, J. S. Szabo, and L. Hangody, "Primary stability of osteochondral grafts used in mosaicplasty," *Arthroscopy* **22,** 414–21 (2006).

[85] R. Korhonen, M. Laasanen, J. Töyräs, R. Lappalainen, H. Helminen, and J. Jurvelin, "Fibril reinforced poroelastic model predicts specifically mechanical behavior of normal, proteoglycan depleted

and collagen degraded articular cartilage," *J Biomech* **36,** 1373–1379 (2003).

[86] J. Krautkramer and H. Krautkramer, *Ultrasonic testing of materials* (Springer, Heidelberg, 1990).

[87] P. C. Kreuz, C. Erggelet, M. R. Steinwachs, S. J. Krause, A. Lahm, P. Niemeyer, N. Ghanem, M. Uhl, and N. Sudkamp, "Is microfracture of chondral defects in the knee associated with different results in patients aged 40 years or younger?," *Arthroscopy* **22,** 1180–6 (2006).

[88] M. S. Laasanen, S. Saarakkala, J. Töyräs, J. Rieppo, and J. S. Jurvelin, "Site-specific ultrasound reflection properties and superficial collagen content of bovine knee articular cartilage," *Phys Med Biol* **50,** 3221–3233 (2005).

[89] M. S. Laasanen, J. Töyräs, J. Hirvonen, S. Saarakkala, R. K. Korhonen, M. T. Nieminen, I. Kiviranta, and J. S. Jurvelin, "Novel mechano-acoustic technique and instrument for diagnosis of cartilage degeneration," *Physiol Meas* **23,** 491–503 (2002).

[90] M. S. Laasanen, J. Töyräs, A. Vasara, S. Saarakkala, M. M. Hyttinen, I. Kiviranta, and J. S. Jurvelin, "Quantitative ultrasound imaging of spontaneous repair of porcine cartilage," *Osteoarthritis Cartilage* **14,** 258–263 (2006).

[91] C.-L. Lee, M.-H. Huang, C.-Y. Chai, C.-H. Chen, J.-Y. Su, and Y.-C. Tien, "The validity of in vivo ultrasonographic grading of osteoarthritic femoral condylar cartilage: a comparison with in vitro ultrasonographic and histologic gradings," *Osteoarthritis Cartilage* **16,** 352–358 (2008).

[92] G. H. Lo, M. LaValley, T. McAlindon, and D. T. Felson, "Intra-articular hyaluronic acid in treatment of knee osteoarthritis: a meta-analysis," *Jama* **290,** 3115–21 (2003).

[93] T. Lyyra, I. Kiviranta, U. Väätäinen, H. J. Helminen, and J. S. Jurvelin, "In vivo characterization of indentation stiffness of articular cartilage in the normal human knee," *J Biomed Mater Res* **48,** 482–7 (1999).

[94] A. J. MacGregor, L. Antoniades, M. Matson, T. Andrew, and T. D. Spector, "The genetic contribution to radiographic hip osteoarthritis in women: results of a classic twin study," *Arthritis Rheum* **43,** 2410–6 (2000).

[95] H. J. Mankin and L. Lippiello, "Biochemical and metabolic abnormalities in articular cartilage from osteo-arthritic human hips," *J Bone Joint Surg Am* **52,** 424–34. (1970).

[96] H. J. Mankin and A. Z. Thrasher, "Water content and binding in normal and osteoarthritic human cartilage," *J Bone Joint Surg Am* **57,** 76–80. (1975).

[97] R. W. Mann, "Comment on 'ultrasonic measurement of the thickness of human articular cartilage in situ' by Yao and Seedhom," *Rheumatology (Oxford)* **40,** 829–31 (2001).

[98] A. Maroudas and M. Venn, "Chemical composition and swelling of normal and osteoarthrotic femoral head cartilage. II. Swelling," *Ann Rheum Dis* **36,** 399–406. (1977).

[99] A. I. Maroudas, "Balance between swelling pressure and collagen tension in normal and degenerate cartilage," *Nature* **260,** 808–9. (1976).

[100] J. A. Martin and J. A. Buckwalter, "Post-traumatic osteoarthritis: the role of stress induced chondrocyte damage," *Biorheology* **43,** 517–21 (2006).

[101] O. Mathiesen, L. Konradsen, S. Torp-Pedersen, and U. Jorgensen, "Ultrasonography and articular cartilage defects in the knee: an in vitro evaluation of the accuracy of cartilage thickness and defect size assessment," *Knee Surg Sports Traumatol Arthrosc* **12,** 440–442 (2004).

[102] M. C. Mensor and M. Scheck, "Follow-up notes on articles previously published in the Journal. Review of six years' experience with the hanging-hip operation," *J Bone Joint Surg Am* **50,** 1250–4 (1968).

[103] G. Merle d'Aubrigné and M. Postel, "Functional results of hip arthroplasty with acrylic prosthesis," *J Bone Joint Surg* **36,** 451–75 (1968).

[104] R. J. Minns, F. S. Steven, and K. Hardinge, "Osteoarthrotic articular cartilage lesions of the femoral head observed in the scanning electron microscope," *J Pathol* **122,** 63–70 (1977).

[105] K. Mithoefer, J. M. Scopp, and B. R. Mandelbaum, "Articular cartilage repair in athletes," *Instr Course Lect* **56,** 457–68 (2007).

[106] K. Mithoefer, r. Williams, R. J., R. F. Warren, H. G. Potter, C. R. Spock, E. C. Jones, T. L. Wickiewicz, and R. G. Marx, "The microfracture technique for the treatment of articular cartilage lesions in the knee. A prospective cohort study," *J Bone Joint Surg Am* **87,** 1911–20 (2005).

[107] K. Mithoefer, r. Williams, R. J., R. F. Warren, T. L. Wickiewicz, and R. G. Marx, "High-impact athletics after knee articular cartilage repair: a prospective evaluation of the microfracture technique," *Am J Sports Med* **34,** 1413–8 (2006).

[108] V. C. Mow, D. C. Fithian, and M. A. Kelly, "Fundamentals of articular cartilage and meniscus biomechanics," in *Articular cartilage and knee joint function: basic science and arthroscopy*, J. W. Ewing, ed. (Raven Press Ltd., New York, 1990).

[109] V. C. Mow, A. Ratcliffe, and A. R. Poole, "Cartilage and diarthrodial joints as paradigms for hierarchical materials and structures," *Biomaterials* **13,** 67–97 (1992).

[110] S. L. Myers, K. Dines, D. A. Brandt, K. D. Brandt, and M. E. Albrecht, "Experimental assessment by high frequency ultrasound of articular cartilage thickness and osteoarthritic changes," *J Rheumatol* **22,** 109–16 (1995).

[111] E. Naredo, C. Acebes, I. Moller, F. Canillas, J. J. de Agustin, E. de Miguel, E. Filippucci, A. Iagnocco, C. Moragues, R. Tuneu, J. Uson, J. Garrido, E. Delgado-Baeza, and I. Saenz-Navarro, "Ultrasound validity in the measurement of knee cartilage thickness," *Ann Rheum Dis* **68,** 1322–7 (2009).

[112] P. Niemeyer, J. Pestka, C. Erggelet, M. Steinwachs, G. Salzmann, and N. Südkamp, "Comparison of arthroscopic and open assessment of size and grade of cartilage defects of the knee," *Arthroscopy* **27,** 46–51 (2011).

[113] H. J. Nieminen, *Acoustic properties of articular cartilage: effect of composition, structure and mechanical loading* (University of Kuopio, Kuopio, Finland, 2007).

[114] H. J. Nieminen, S. Saarakkala, M. S. Laasanen, J. Hirvonen, J. S. Jurvelin, and J. Töyräs, "Ultrasound attenuation in normal and spontaneously degenerated articular cartilage," *Ultrasound Med Biol* **30,** 493–500 (2004).

[115] H. J. Nieminen, J. Töyräs, M. S. Laasanen, and J. S. Jurvelin, "Acoustic properties of articular cartilage under mechanical stress," *Biorheology* **43,** 523–535 (2006).

[116] H. J. Nieminen, J. Töyräs, J. Rieppo, M. T. Nieminen, J. Hirvonen, R. Korhonen, and J. S. Jurvelin, "Real-time ultrasound analysis of articular cartilage degradation in vitro," *Ultrasound Med Biol* **28,** 519–525 (2002).

[117] H. J. Nieminen, Y. Zheng, S. Saarakkala, Q. Wang, J. Töyräs, Y. Huang, and J. Jurvelin, "Quantitative assessment of articular cartilage using high-frequency ultrasound: research findings and diagnostic prospects," *Crit Rev Biomed Eng* **37,** 461–94 (2009).

[118] M. T. Nieminen, J. Töyräs, J. Rieppo, J. M. Hakumäki, J. Silvennoinen, H. J. Helminen, and J. S. Jurvelin, "Quantitative MR microscopy of enzymatically degraded articular cartilage," *Magn Reson Med* **43,** 676–81 (2000).

[119] R. A. Nishimura, W. D. Edwards, C. A. Warnes, G. S. Reeder, J. Holmes, D. R., A. J. Tajik, and P. G. Yock, "Intravascular ultrasound imaging: in vitro validation and pathologic correlation," *J Am Coll Cardiol* **16,** 145–54 (1990).

[120] S. E. Nissen and P. Yock, "Intravascular ultrasound: novel pathophysiological insights and current clinical applications," *Circulation* **103,** 604–16 (2001).

[121] S. P. Oakley, P. I., Z. Szomor, A. Turnbull, G. A. C. Murrell, B. W. Kirkham, and M. N. Lassere, "Accuracy and reliability of arthroscopic estimates of cartilage lesion size in a plastic knee simulation model," *Arthroscopy* **19,** 282–289 (2003).

[122] S. Odenbring, N. Egund, A. Lindstrand, L. S. Lohmander, and H. Willen, "Cartilage regeneration after proximal tibial osteotomy for medial gonarthrosis. An arthroscopic, roentgenographic, and histologic study," *Clin Orthop Relat Res* 210-6 (1992).

[123] S. W. O'Driscoll, F. W. Keeley, and R. B. Salter, "The chondrogenic potential of free autogenous periosteal grafts for biological resurfacing of major full-thickness defects in joint surfaces under the influence of continuous passive motion. An experimental investigation in the rabbit," *J Bone Joint Surg Am* **68,** 1017–35 (1986).

[124] D. J. Ogilvie-Harris and R. W. Jackson, "The arthroscopic treatment of chondromalacia patellae," *J Bone Joint Surg Br* **66,** 660–5 (1984).

[125] H. K. Outerbridge, A. R. Outerbridge, and R. E. Outerbridge, "The use of a lateral patellar autologous graft for the repair of a large osteochondral defect in the knee," *J Bone Joint Surg Am* **77,** 65–72 (1995).

[126] A. Ozturk, M. R. Ozdemir, and Y. Ozkan, "Osteochondral autografting (mosaicplasty) in grade IV cartilage defects in the knee joint: 2- to 7-year results," *Int Orthop* **30,** 200–4 (2006).

[127] B. Pellaumail, V. Dewailly, A. Watrin, D. Loeuille, P. Netter, G. Berger, and A. Saïed, "Attenuation coefficient and speed of sound in immature and mature rat cartilage: a study in the 30-70 MHz frequency range," *IEEE Ultrasonics Symposium.* 1361-1365 (1999).

[128] B. Pellaumail, A. Watrin, D. Loeuille, P. Netter, G. Berger, P. Laugier, and A. Saied, "Effect of articular cartilage proteoglycan depletion on high frequency ultrasound backscatter," *Osteoarthritis Cartilage* **10,** 535–541 (2002).

[129] J. P. Pelletier and J. Martel-Pelletier, "DMOAD developments: present and future," *Bull NYU Hosp Jt Dis* **65,** 242–8 (2007).

[130] A. G. Podoleanu, "Optical coherence tomography," *Br J Radiol* **78,** 976–88 (2005).

[131] B. N. Potkin, A. L. Bartorelli, J. M. Gessert, R. F. Neville, Y. Almagor, W. C. Roberts, and M. B. Leon, "Coronary artery imaging with intravascular high-frequency ultrasound," *Circulation* **81,** 1575–85 (1990).

[132] H. Pulkkinen, V. Tiitu, P. Valonen, T. Silvast, J. Jurvelin, J. Töyräs, M. Lammi, and I. Kiviranta, "Repair of osteochondral defects with recombinant human type II collagen gel and autologous chondrocytes in rabbit model," *56th Annual Meeting, Orthopaedic Research Society, New Orleans* (2010).

[133] P. Qvist, A.-C. Bay-Jensen, C. Christiansen, E. Dam, P. Pastoureau, and M. Karsdal, "The disease modifying osteoarthritis drug (DMOAD): Is it in the horizon?," *Pharmacol Res* **58,** 1–7 (2008).

[134] E. Radin and R. Rose, "Role of subchondral bone in the initiation and progression of cartilage damage," *Clin Orthop Relat Res.* **213,** 34–40 (1986).

[135] E. L. Radin, P. Maquet, and H. Parker, "Rationale and indications for the "hanging hip" procudure: a clinical and experimental study," *Clin Orthop Relat Res* 221-30 (1975).

[136] J. Rieppo, J. Hallikainen, J. S. Jurvelin, I. Kiviranta, H. J. Helminen, and M. M. Hyttinen, "Practical considerations in the use of polarized light microscopy in the analysis of the collagen network in articular cartilage," *Microsc Res Tech* **71,** 279–87 (2008).

[137] J. Rieppo, J. Töyräs, M. T. Nieminen, V. Kovanen, M. M. Hyttinen, R. K. Korhonen, J. S. Jurvelin, and H. J. Helminen, "Structure-function relationships in enzymatically modified articular cartilage," *Cells Tissues Organs* **175,** 121–32 (2003).

[138] S. Saarakkala, R. K. Korhonen, M. Laasanen, J. Töyräs, J. Rieppo, and J. S. Jurvelin, "Mechano-acoustic determination of Young's modulus of articular cartilage," *Biorheology* **41,** 167–179 (2004).

[139] S. Saarakkala, M. Laasanen, J. Töyräs, and J. S. Jurvelin, "Quantitative ultrasound imaging detects articular cartilage and subchondral bone changes in spontaneous cartilage degeneration," (2006).

[140] S. Saarakkala, M. S. Laasanen, J. S. Jurvelin, K. Törrönen, M. J. Lammi, R. Lappalainen, and J. Töyräs, "Ultrasound indentation of normal and spontaneously degenerated bovine articular cartilage," *Osteoarthritis Cartilage* **11,** 697–705 (2003).

[141] S. Saarakkala, S. Z. Wang, Y. P. Huang, and Y. P. Zheng, "Quantification of the optical surface reflection and surface roughness of articular cartilage using optical coherence tomography," *Phys Med Biol* **54,** 6837–52 (2009).

[142] A. Saïed, E. Chérin, H. Gaucher, P. Laugier, P. Gillet, J. Floquet, P. Netter, and G. Berger, "Assessment of articular cartilage and subchondral bone: subtle and progressive changes in experimental osteoarthritis using 50 MHz echography in vitro," *J Bone Miner Res* **12,** 1378–1386 (1997).

[143] M. Scheck, "Roentgenographic changes of the hip joint following extra-articular operations for degenerative arthritis," *J Bone Joint Surg Am* **52,** 99–104 (1970).

[144] N. Shasha, S. Krywulak, D. Backstein, A. Pressman, and A. E. Gross, "Long-term follow-up of fresh tibial osteochondral allografts for failed tibial plateau fractures," *J Bone Joint Surg Am* **85-A Suppl 2,** 33–9 (2003).

[145] L. S. Simon, "Osteoarthritis: A Review," *Office rheumatology* **2,** 26–36 (1999).

[146] C. Slemenda, K. D. Brandt, D. K. Heilman, S. Mazzuca, E. M. Braunstein, B. P. Katz, and F. D. Wolinsky, "Quadriceps weakness and osteoarthritis of the knee," *Ann Intern Med* **127,** 97–104 (1997).

[147] G. Spahn, H. Klinger, and G. Hofmann, "How valid is the arthroscopic diagnosis of cartilage lesions? Results of an opinion survey among highly experienced arthroscopic surgeons," *Arch Orthop Trauma Surg* (2009).

[148] J. Steadman, W. Rodkey, S. Singleton, and K. Briggs, "Microfracture technique for full-thickness chondral defects: Technique and clinical results.," *Operat Techn Orthop* **7,** 300–304 (1997).

[149] P. Stepanishen, "The Time-Dependent Force and Radiation Impedance on a Piston in a Rigid Infinite Planar Baffle," *J. Acoust. Soc. Am.* **49,** 841–849 (1970).

[150] P. H. Tomlins and R. K. Wang, "Theory, developments and applications of optical coherence tomography," *J. Phys. D: Appl. Phys.* 2519-2535 (2005).

[151] G. E. Tupholme, "Generation of acoustic pulses by baffled plane pistons," *Mathematika* **16,** 209–224 (1969).

[152] J. Töyräs, M. S. Laasanen, S. Saarakkala, M. J. Lammi, J. Rieppo, J. Kurkijärvi, R. Lappalainen, and J. S. Jurvelin, "Speed of sound in normal and degenerated bovine articular cartilage," *Ultrasound Med Biol* **29,** 447–454 (2003).

[153] J. Töyräs, J. Rieppo, M. Nieminen, H. Helminen, and J. Jurvelin, "Experimental characterisation of enzymatically induced degeneration of articular cartilage using high frequency ultrasound," (1999).

[154] J. Töyräs, J. Rieppo, M. T. Nieminen, H. J. Helminen, and J. S. Jurvelin, "Characterization of enzymatically induced degradation of articular cartilage using high frequency ultrasound," *Phys Med Biol* **44,** 2723–2733 (1999).

[155] M. Venn and A. Maroudas, "Chemical composition and swelling of normal and osteoarthrotic femoral head cartilage. I. Chemical composition," *Ann Rheum Dis* **36,** 121–9 (1977).

[156] T. Virén, S. Saarakkala, E. Kaleva, H. J. Nieminen, J. S. Jurvelin, and J. Töyräs, "Minimally invasive ultrasound method for intra-articular diagnostics of cartilage degeneration," *Ultrasound Med Biol* **35,** 1546–1554 (2009).

[157] Q. Wang, Y. Zheng, X. Wang, Y. Huang, M. Liu, S. Z. Wang, Z. Zhang, and X. Guo, "Ultrasound evaluation of site-specific effect of simulated microgravity on articular cartilage," *Ultrasound Med Biol* **36,** 1086–1097 (2010).

[158] Q. Wang, Y. P. Zheng, G. Leung, W. L. Lam, X. Guo, H. B. Lu, L. Qin, and A. F. T. Mak, "Altered osmotic swelling behavior of proteoglycan-depleted bovine articular cartilage using high frequency ultrasound," *Phys Med Biol* **53,** 2537–2552 (2008).

[159] S. Wang, Y. Huang, S. Saarakkala, and Y. Zheng, "Quantitative assessment of articular cartilage with morphologic, acoustic and mechanical properties obtained using high-frequency ultrasound," *Ultrasound Med Biol* **36,** 512–527 (2010).

[160] D. P. Weigel and J. L. Marsh, "High-energy fractures of the tibial plateau. Knee function after longer follow-up," *J Bone Joint Surg Am* **84-A,** 1541–51 (2002).

[161] H. Weisl, "Intertrochanteric osteotomy for osteoarthritis. A long-term follow-up," *J Bone Joint Surg Br* **62-B,** 37–42 (1980).

[162] P. N. T. Wells, *Physical principles of ultrasonic diagnosis*, Vol. 1 of *Medical physics* (Academic Press Inc., New York, 1969).

[163] J. E. Wilhjelm, P. C. Pedersen, and S. M. Jacobsen, "The Influence of Roughness, Angle, Range, and Transducer Type on the Echo Signal from Planar Interfaces," *IEEE Trans Ultrason Ferroelectr Freq Control* **48,** 511–521 (2001).

[164] T. Xie, S. Guo, J. Zhang, Z. Chen, and G. M. Peavy, "Determination of characteristics of degenerative joint disease using optical coherence tomography and polarization sensitive optical coherence tomography," *Lasers Surg Med* **38,** 852–65 (2006).

[165] J. Q. Yao and B. B. Seedhom, "Ultrasonic measurement of the thickness of human articular cartilage in situ," *Rheumatology* **38,** 1269–71 (1999).

[166] J. Yin, H. Yang, X. Li, J. Zhang, Q. Zhou, C. Hu, K. Shung, and Z. Chen, "Integrated intravascular optical coherence tomography ultrasound imaging system," *J Biomed Opt* **15** (2010).

[167] J. Yu and B. W. D., "Osteochondral allograft trasnplantation," in *Cartilage repair strategies*, R. J. Williams, ed. (New Jersey: Humana press, 2007).

[168] K. Zaslav, B. Cole, R. Brewster, T. DeBerardino, J. Farr, P. Fowler, and C. Nissen, "A prospective study of autologous chondrocyte implantation in patients with failed prior treatment for articular cartilage defect of the knee: results of the Study of the Treatment of Articular Repair (STAR) clinical trial," *Am J Sports Med* **37,** 42–55 (2009).

[169] J. Zemanek, "Beam behavior within the nearfield of a vibrating piston," *J. Acoust. Soc. Am.* **49,** 181–191 (1971).

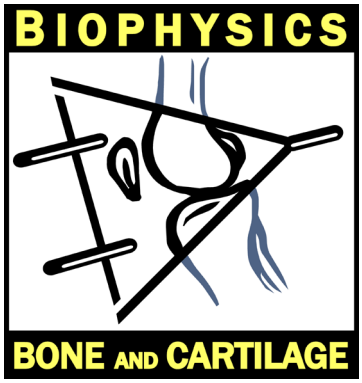

Tuomas Virén

Arthroscopic Ultrasound Imaging of Articular Cartilage

Quantitative ultrasound imaging is a method for evaluation of the integrity of articular cartilage and subchondral bone. However, no ultrasound technique capable for arthroscopic imaging of articular cartilage has been introduced. The aim of this study was to investigate the potential of an ultrasound technique, based on the use of a clinical intravascular ultrasound device, for arthroscopic imaging of articular cartilage. The technique provided quantitative information on the degenerative status of articular cartilage and was found to be suitable for evaluation of integrity of cartilage repair. Importantly, the technique was clinically applicable and provided diagnostically valuable information.

UNIVERSITY OF
EASTERN FINLAND

Publications of the University of Eastern Finland
Dissertations in Forestry and Natural Sciences

ISBN 978-952-61-0470-6